

***In Vitro* Metabolism of 6-Chloro-9-(4-methoxy-3,5-dimethylpyridin-2-ylmethyl)-9H-purin-2-ylamine (BIIB021), an Inhibitor of HSP90, in Liver Microsomes and Hepatocytes of Rats, Dogs, and Humans and Recombinant Human Cytochrome P450 Isoforms**

Lin Xu, Caroline Woodward, Samina Khan, Chandra Prakash

Drug Metabolism and Preclinical Safety, Biogen Idec, Cambridge, MA, 02142

Running Title: Metabolism of a pyridinylmethyl-9H-purin-2-ylamine analog

Corresponding author: Lin Xu, Drug Metabolism and Preclinical Safety, Biogen Idec,
Cambridge, MA, 02142. Phone number: (617) 914-7191; Fax number: (617) 679-3463;
E-mail address: Lin.xu@biogenidec.com

Text pages: 26

Tables: 3

Figures: 11

References: 25

Abstract: 273

Introduction: 509

Discussion: 1273

Abbreviations: HSP, heat shock protein; RAM, Radioactivity monitor; ARC, accurate radioisotope counting; CYP450, cytochrome P450;; GSH, glutathione; HPLC, high performance liquid chromatography; HR: high resolution; LC, liquid chromatography; MS, mass spectrometry; NAD, nicotinamide adenine dinucleotide; NADPH, nicotinamide adenine dinucleotide phosphate.

Abstract

Inhibition of heat shock protein 90 (HSP90) results in the degradation of oncoproteins that drive malignant progression and induce cell death, thus making HSP90 a potential target of cancer therapy. 6-Chloro-9-(4-methoxy-3, 5-dimethyl-pyridin-2-ylmethyl)-9H-purin-2-ylamine (BIIB021), a synthetic HSP90 inhibitor, exhibited promising antitumor activity in preclinical models. It is currently in phase II clinical trials for the oral treatment of breast cancer. The objective of this study was to obtain both quantitative and qualitative metabolic profiles of [¹⁴C]BIIB021 in rat, dog and human liver microsomes and hepatocytes to provide support for *in vivo* safety and clinical studies. The metabolites of [¹⁴C]BIIB021 were identified using LC-MS/MS coupled with radiometric detection. BIIB021 was extensively metabolized in both liver microsomes and hepatocytes. The major oxidative metabolic pathways identified for all species were due to hydroxylation (M7) and *O*-demethylation (M2) of the methoxy-dimethylpyridine moiety. Majority of M7 in dog hepatocytes was further conjugated to form the glucuronide (M4). Oxidative dechlorination (M6), monooxygenation (M10) and oxidative *N*-dealkylation of the methoxy-dimethylpyridine moiety (M11 and M12) were observed as the minor metabolic pathways in hepatocytes of all three species. A glutathione conjugate (M18) was also identified in all species. Its formation was catalyzed, in part, by soluble glutathione S-transferase via direct displacement of the chlorine on the amino-chloropurine moiety. Subsequent minor secondary metabolites M13, M14, M15 and M17 were observed in human, dog, and rat hepatocytes. Results from incubations of BIIB021 with human recombinant CYP450 isoforms and CYP450 antibody inhibition study in human liver microsomes suggested that the formation of M7

is mainly catalyzed by CYP2C19 and CYP3A4 while the formation of minor metabolite M2 in human liver microsomes probably attributes to CYP3A4.

Introduction

Heat shock protein 90 (HSP90) is an abundant molecular chaperone that promotes the conformational maturation of ‘client’ proteins and protects them from degradation (Biamonte *et al.*, 2010; Pearl *et al.*, 2006; Soo *et al.*, 2008). Many of the known clients are protein kinase or transcription factors involved in multiple signal transduction pathways. HSP90 is also expressed in the activated form in cancer cells, whereas it was latent in normal somatic cells. Therefore, it has become an attractive target in oncology. Inhibition of HSP90 function causes many oncogenic client proteins to adopt aberrant conformations and subsequent degradation. Therefore, HSP90 inhibitors represent a promising approach to treat cancers driven by multiple molecular abnormalities.

BIIB021, 6-chloro-9-(4-methoxy-3,5-dimethylpyridin-2-yl)methyl-9H-purin-2-ylamine, is a synthetic HSP90 inhibitor and exhibited a strong antitumor effect as a single agent and increased the efficacy of radiation (Kasibhatla *et al.*, 2007; Lundgren *et al.*, 2009). Orally-administered BIIB021 demonstrated efficacy in the U87 glioblastoma, the N87 gastric carcinoma, and the BT474 breast carcinoma xenograft models in nude mice. The combinations of BIIB021 with paclitaxel or bortezomib demonstrated significant tumor growth inhibition compared with single-agent treatment or controls in ovarian tumor and myeloma xenograft models, respectively. It also synergizes with radiation, a commonly used therapy in the treatment of squamous cell carcinoma. BIIB021 is not a substrate of p-glycoprotein and showed comparable potency against MDR expression cell line (Zhang *et al.*, 2010). It is under development as an oral agent for the treatment of breast cancer.

Identification of metabolites of a new chemical entity (NCE) in animals and humans is essential to pharmaceutical development and compound progression. The Food and Drug administration (FDA) recommends that the metabolic profiles of all NCEs in humans should be characterized before initiating large clinical trials. *In vitro* studies using preclinical species and human hepatocellular and subcellular fractions and/or recombinant human enzymes often provide valuable information on the metabolic pathways in humans *in vivo* (Baranczewski *et al.*, 2006; Dalvie *et al.*, 2009). The illustrated metabolic pathways *in vitro* in animals and humans also provide guidance to select the right animal species for long-term safety assessment studies, and to ensure that the selected animal species are exposed to all major metabolites formed in humans (Baillie *et al.*, 2002; FDA, 2008).

BIIB021 is rapidly absorbed *in vivo* and has a short half-life in mouse (Kasibhatla *et al.*, 2007), rat, and dog. It shows moderate or high clearance in these animal species. The elimination of BIIB021 is likely through metabolism (Xu *et al.*, 2010). The objectives of this study were to obtain both quantitative and qualitative metabolite profiles of [¹⁴C]BIIB021 after incubations in rat, dog, and human liver microsomes and hepatocytes. The metabolites were characterized by high resolution LC-MS/MS and by comparisons of their retention times on HPLC, and MS spectra with those of the synthetic standards. In addition, incubations using cDNA-expressed human CYP450s were performed to determine the CYP450s responsible for the formation of major oxidative metabolites (M2 and M7). The role of cytosolic enzymes such as aldehyde oxidase (AO) and glutathione S-transferase (GST) on metabolism of BIIB021 was also investigated.

Materials and Methods

Reference Compounds and Chemicals BIIB021, [^{14}C]BIIB021, and authentic standards, CF2246 (*O*-desmethyl BIIB021, 2-((2-amino-6-chloro-9H-purin-9-yl)methyl)-3,5-dimethylpyridin-4-ol, M2), 5-OH-1983 Gluc (5-hydroxymethyl glu, M4), and CF3785 (5-hydroxymethyl BIIB021, (6-((2-amino-6-chloro-9H-purin-9-yl)methyl)-4-methoxy-5-methylpyridin-3-yl)methanol, M7), and CF2483 (2-amino-6-chloro-9-((4-methoxy-3,5-dimethylpyridin-2-yl)methyl)-9H-purin-8-ol, M10) were synthesized at Biogen Idec (Kasibhatla *et al.*, 2005; Kasibhatla *et al.*, 2007).

The ^{14}C -label was incorporated on the C-8 position of the purine ring (Fig.1). It had a specific activity of 52.9 mCi/mmol and a radiochemical purity of >99%, as determined by HPLC using an in-line radioactivity detector. 7-chloro-1H-[1,2,3]triazolo[4,5-d]pyrimidin-5-amine was purchased from TCI America (Portland, OR). Allupurinol, ethacrynic acid, isovanillin, menadione, and raloxifene were purchased from Sigma-Aldrich (St. Louis, MO). All other chemicals were HPLC or analytical grade and were obtained from Fisher Scientific (Suwanee, GA), unless specified otherwise.

Pooled liver microsomes (20 mg/ml) of Sprague Dawley rats, Beagle dogs, and humans were purchased from XenoTech (Lenexa, Kansas). The pooled human liver microsomes (lot #910251) consisted of liver samples from 50 donors of both genders. Ten donor (five male, five female) pooled human cryopreserved hepatocytes were purchased from CellzDirect (Austin, TX). For the rat or dog, male and female cryopreserved hepatocytes were ordered from CellzDirect and pooled first before the incubation with BIIB021.

Microsomes from baculovirus-infected Sf9 insect cells expressing CYP450 reductase and each individual human CYP450 were purchased from BD Bioscience (Bedford, MA).

The monoclonal antibodies against CYP1A2, CYP2A6, CYP2B6, CYP2C19, CYP2D6, CYP2E1, and CYP3A4 were also purchased from BD Bioscience.

Microsomal, Cytosolic, and Recombinant human CYP450s Incubations

Metabolism of BIIB021 was studied in duplicate in rat, dog, and human liver microsomal (LM) and cytosolic subcellular fractions and recombinant human CYP450s. For liver microsomes, the incubation mixture (300 μ L in the total volume) consisted of the following components: 1 mg/ml of microsomal protein, 10 μ M [14 C]BIIB021, 0.5 μ Ci/mL (diluted from 100 μ M, 5 μ Ci/mL test solution), 1 mM NADPH, 3.3 mM MgCl₂, 100 mM potassium phosphate, pH 7.4. Reactions were started by adding NADPH (final concentration at 1 mM) and incubated at 37°C in shaking incubator block (450 rpm). After 90 min, reactions were terminated with 300 μ L of ice-cold acetonitrile containing 0.1% formic acid. Control incubations were performed without NADPH. Samples were then centrifuged; supernatants were directly analyzed by LC-RAM-MS.

For the liver cytosolic incubations, the mixtures contained 1 mg/mL human cytosolic protein and 10 μ M [14 C]BIIB021 (0.5 μ Ci/mL) in a final volume of 500 μ L of 100 mM phosphate buffer (pH 7.4). The reaction was quenched with ice-cold acetonitrile (500 μ L) after 30 min incubation. The quenched reaction mixture was vortexed and centrifuged for 10 min at 4°C. The supernatant was directly analyzed by LC-MS. In the inhibition studies, aldehyde/xanthine oxidase selective inhibitors, isovanillin (100 μ M),

menadione (100 μ M), allopurinol (100 μ M), and raloxifene (50 μ M) were preincubated in human liver cytosol for 10 min at 37°C before the addition of BIIB021.

In the recombinant human CYP450 incubations, the mixtures (300 μ L) contained microsomes (50 pmol/mL) from baculovirus-infected Sf9 insect cells and 10 μ M (0.5 μ Ci/mL) [14 C]BIIB021 in a 100 mM potassium phosphate buffer (pH 7.4). The incubations were initiated by adding the NADPH with final concentration at 1 mM. The mixture was incubated with gentle shaking for 30 min at 37°C and terminated by adding 300 μ L of ice-cold acetonitrile containing 0.1% formic acid. Samples were processed same as above before LC-MS analysis. Incubations were conducted in duplicates and expressed human CYP450s include CYP1A2, CYP2A6, CYP2C8, CYP2C9, CYP2C19, CYP2D6, and CYP3A4.

In the glutathione fortified incubations, 300 μ L mixtures contained 10 μ M [14 C]BIIB021 (0.5 μ Ci/mL) and 1 mg/ml enzymes (either human liver microsomes or cytosols) in 100 mM potassium phosphate buffer at pH 7.4. Reactions were started by adding GSH (final concentration at 10 mM) or water in controls. GST inhibitor ethacrynic acid (100 μ M) was pre-treated with incubation mixture for five min before adding BIIB021. After 90 min incubations, reactions were terminated with 300 μ L of ice-cold acetonitrile. Samples were processed same as above before LC-MS analysis.

HLM Incubations in the Presence of CYP Monoclonal Antibody

For liver microsomes, the incubation mixture (300 μ L in the total volume) consisted of the following components: 1 mg/ml of microsomal protein, 10 μ M [14 C]BIIB021, 0.5 μ Ci/mL (diluted from 100 μ M, 5 μ Ci/mL test solution), 1 mM NADPH, 3.3 mM MgCl₂, 100 mM potassium phosphate, pH 7.4. Reactions were started

by adding NADPH (final concentration at 1 mM) and incubated at 37°C in shaking incubator block (450 rpm). After 90 min, reactions were terminated with 300 µL of ice-cold acetonitrile containing 0.1% formic acid. Control incubations were performed without NADPH. Samples were then centrifuged; supernatants were directly analyzed by LC-RAM-MS.

The incubations were conducted in duplicate at a final volume of 300 µL. Each reaction mixture consisted of human liver microsomal proteins (1 mg/ml), 10 µM [¹⁴C]BIIB021 (0.5 µCi/mL), 1 mM NADPH, 3.3 mM MgCl₂, and 15 µL anti-CYP antibodies in phosphate buffer (100 mM, pH 7.4). Incubations without antibody were conducted as the positive controls. All components except BIIB021 and NADPH were mixed and preincubated for 15 min on ice, and then 5 min at 37°C. BIIB021 and NADPH were added and the mixture was incubated for additional 60 min at 37°C. The mixture was quenched with 300 µL of ice-cold acetonitrile containing 0.1% formic acid. The samples were then centrifuged; supernatants were directly analyzed by LC-RAM to determine the concentration of M7. In order to achieve maximum inhibition of M7 formation, different volume of anti-CYP2C19 and anti-CYP3A4 was used in the human liver microsomal incubations.

Hepatocyte Incubations

Metabolism of [¹⁴C]BIIB021 was evaluated in rat, dog and human hepatocytes. Incubations were performed in duplicates in Krebs-Henseleit buffer. The final substrate concentration in cell suspension was 10 µM (0.5 µCi/mL) in a volume of 0.5 mL at a cell density of 1 x 10⁶ cells/mL. Incubations proceeded for 1.5 h at 37 °C in the 24-well incubation plate under 95% O₂:5% CO₂. 7-Ethoxycoumarin was incubated as a positive

control for the hepatocytes. To ensure maximum recovery of compound, 10 μ L aliquot of each incubation mixture was added to 5 mL of scintillation fluid before quenching the reaction. The samples were then quenched with 50 μ L of ice cold trichloroacetic acid and were put on ice. The samples were sonicated for 20 min, vortexed and centrifuged for 20 min. The radioactivity recovery was measured by comparing recovery before terminating reaction and after terminating reaction. The supernatant was then analyzed by LC-RAM-MS.

Instrumentation. The LC-RAM-MS system consisted of an Agilent 1290 Infinity UHPLC system (Santa Clara, CA), a v.ARC radiometric detector (Hockessin, Delaware), and a Thermo LTQ QorbitrapTM high resolution mass spectrometer (San Jose, CA). The separation of metabolites was performed on, a Luna[®] analytical C₁₈ (2) column (4.6 x 150 mm, 3 μ m particle size, Phenomenex, Torrance, CA) with on-line radioactivity monitoring using a mobile phase containing a mixture of 0.4% formic acid in water (pH 3.72; solvent A) and acetonitrile (solvent B). The column was held at 35°C and the samples were eluted at a flow rate of 0.70 mL/min. The mobile phase was initially composed of solvent A/solvent B (100:0) for 3 min. It was then programmed with four subsequent linear gradients (5 min from 0% to 6% B; 5 min from 6% to 10% B; 20 min from 10% to 16% B; 14 min from 16% to 30% B; 8 min from 30% to 100% B), and finally with 5 min at 100% B. It was returned to the starting solvent mixture over 15 min. The system was allowed to equilibrate for approximately 15 min before making the next injection. The HPLC effluent was directly infused into the radiometric detector or mass spectrometer. StopFlow ADTM cocktail (AIM, Hockessin, Delaware) was used as the scintillation liquid. The LTQ QorbitrapTM mass spectrometer was operated in the positive

electrospray ionization mode. The heated capillary temperature was maintained at 250 °C; the sheath gas and auxiliary gas flow rates were set to 60 and 40 units, respectively. The ion spray voltage, capillary voltage, and tube lens offset voltage were adjusted to 3 kV, 40 V and 85 V, respectively. The normalized collision energy was 30% during MS/MS acquisition and helium was used as the collision gas. High resolution mass measurement was performed in OrbitrapTM mode with a resolution of 15K. The instrument was calibrated with a mixture of solution (Thermo, San Jose, CA) containing caffeine, L-methionyl-arginyl-phenylalanyl-alanine acetate, and Ultramark 1621. High resolution data was expressed as four decimal atomic mass units and mass difference (ΔM) between measured mass and the calculated mass was expressed in parts per million (ppm) units. Elemental compositions were calculated based on high resolution mass data and McLafferty's nitrogen rule.

Results

Metabolite Profiles of [¹⁴C]BIIB021 in LM and Hepatocytes

Recovery of radioactivity from all *in vitro* incubations of [¹⁴C]BIIB021 in liver microsomes and hepatocytes was >85%. The supernatant from each incubation mixture was used for radioactivity profiling of metabolites.

The representative HPLC-radiochromatograms of metabolites in rat, dog, and human LM incubations are shown in Fig. 2. The relative percentage of individual radioactivity peak is summarized in Table 1. BIIB021 was moderately stable in liver microsomes at the clinical efficacious concentration of 10 μM. Approximately 66% of [¹⁴C]BIIB021 was biotransformed to metabolites during 90 min incubation in the presence of NADPH. M6 (oxidative dechlorination) was identified as a minor degradant (0.5% to 1%) in the control and buffer (data not shown) incubations. In addition to the parent drug and M6, a total of one non-radioactive and four radioactive metabolites were detected. In rat, dog, and human LM, M2 and M7 were identified as the major metabolites, representing 4.5% and 53% in rat, 9.5% and 36.2% in dog, and 3.6% and 42.2% of the radioactivity in human LM, respectively. Oxidative *N*-dealkylation of the 4-methoxy-3,5-dimethylpyridine moiety M11 and M12 was found as an additional metabolic pathway in rat LM and the resulting metabolites, M11 and M12 represented ~6.9% of the radioactivity. A minor metabolite M10 (mono-hydroxylation, ~1.2%) was also identified in rat, dog, and human LM at 1.3, 0.3, and 0.5% of the radioactivity, respectively.

The representative HPLC-radiochromatograms of metabolites in rat, dog, and human hepatocytes and in buffer are shown in Fig. 3. The relative percentage of

individual radioactivity peak is summarized in Table 2. A total of 12 (11 radioactive and one non-radioactive) metabolites were identified from these incubations. BIIB021 was extensively metabolized in rat and dog hepatocytes and less than 5% and 0.8% of [¹⁴C]BIIB021, remained unchanged in rat and dog, respectively, after 90 min incubations. BIIB021 was relatively stable in human hepatocytes and ~38% remained unchanged after incubation. In rat, dog, and human hepatocytes, M7 was identified as a major metabolite, representing ~37.5%, 3%, and 49% of the radioactivity, respectively. Majority of M7 in dog was further biotransformed to a glucuronide conjugate (M4), representing ~44.8% of radioactivity. M4 represented 10.2% of radioactivity in the rat but was not detected in the human hepatocytes. *O*-Demethylation (M2) was also determined as one of the major metabolic pathway and it represented ~8.7%, 25.5%, and 0.5% of the radioactivity in rat, dog, and human hepatocytes. Consistent with rat LM, oxidative *N*-dealkylation was found only in rat hepatocytes and the resulting metabolites, M11 and M12 both represented ~11.1% of the radioactivity. Several glutathione (GSH) conjugates were also identified in the incubations. M18 representing 13.1% and 9% of radioactivity in rat and dog hepatocytes was formed by direct displacement of the Cl atom by GSH. M14 was a GSH substituted dechlorinated M2, representing ~7% of radioactivity in dog hepatocytes. None of these metabolites was identified in human hepatocytes. M17 was identified as a GSH substituted dechlorinated monohydroxylated BIIB021 and it presented 9.1%, 3%, and 1.8% of radioactivity in rat, dog, and human hepatocytes. M6 and M15, which were formed by oxidative dechlorination of BIIB021 and M7, were found dominant in human hepatocytes, representing 4.4% and 3.4% of radioactivity, respectively. Again, M6 was formed in control Krebs buffer, suggesting that it is, in part, formed non-enzymatically.

A minor metabolite M10 (mono-hydroxylation) was represented only less than 2% of radioactivity across all species. Other metabolites M13 and M16 were formed by combination of these primary pathways. M13 was detected at 1% of radioactivity in dog hepatocytes. M16 (purine oxidation and *O*-demethylation), accounting for 1.9% of the radioactivity, was found only in human hepatocytes.

Metabolite Identification and Characterization

A total of 13 metabolites were identified in liver microsomes and hepatocytes incubations by high resolution LC-MS/MS. BIIB021 contains one chlorine atom that has two major isotopes, ^{35}Cl and ^{37}Cl , in a natural abundance ratio of ca. 3 to 1. Retention time of radioactive peaks in chromatograms and the characteristic $^{35}/^{37}\text{Cl}$ ion clusters observed in LC/MS data were used to find and confirm the molecular ions of BIIB021 and its metabolites that retained the chlorine atom. The [^{14}C]BIIB021 has a high percentage in the incubation solution with a ratio of [^{12}C]BIIB021 to [^{14}C] BIIB021 close to 1:3. Therefore, the $^{12}\text{C}/^{14}\text{C}$ ion clusters along with chlorine pattern observed in the LC/MS data were also used for detecting metabolites and interpreting their fragmentation patterns in MS/MS spectra. The structures of each metabolite were elucidated by interpreting the mass change of molecular ion and similarity/change of fragmentation patterns, compared with those of BIIB021. The exact location of modification in major metabolites was determined by comparing the retention time, elemental composition, and product ion spectra of available synthetic standards.

BIIB021 eluted at ~47.98 min on HPLC and produced protonated molecular ions at m/z 319/321/323 at the ratio of 1:3.3:1.1. The product ion (MS/MS) spectrum of BIIB021 with proposed characteristic fragmentations is displayed in Fig. 4. Loss of an HCl molecule resulted in the product ion at m/z 283, which gave a product ion at m/z 268 via further loss of a methyl group. The product ions at m/z 302/304 were formed from the loss of an NH_3 (-17 Da). Other characteristic ion at m/z 150 is formed by cleavage of the C-N bond between the purine moiety and the pyridine ring with charge retention at the pyridine moiety. The subsequent loss of the formaldehyde from ion at m/z 150 produced a fragment at m/z 120. The characteristic ions at m/z 150 and 120 proved to be very useful for finding and confirming the structural changes of BIIB021 and its metabolites that retained the intact pyridine ring.

Metabolite M2 was detected in all three species. It eluted at ca. 23.74 min on HPLC and produced protonated molecular ions at m/z 305/307. The product ions at m/z 269/271 were formed from loss of an HCl molecule (-36 Da). The product ions at m/z 170/172 and 136 corresponded to the 2-amino-4-chlorine-purine moiety and the pyridine ring moiety, respectively (Supplemental Figure 1). The 14 Da loss from pyridine ring moiety suggested that M2 was an *O*-desmethyl metabolite of BIIB021. M2 also has the same HPLC retention time and product ion spectra to those of the reference standard, 2-(2-amino-6-chloro-9H-purin-9-yl)methyl-3,5-dimethylpyridin-4-ol (CF2246). Therefore, M2 was identified as *O*-desmethyl BIIB021.

Metabolite M4 was detected in rat and dog hepatocyte incubations. It eluted at ca. 27.23 min and produced protonated molecular ions at m/z 511/513. The product ions at m/z 335/337 (Supplemental Figure 2) corresponded to loss of a glucuronic acid moiety (-

176 Da). This aglycone had 16 Da higher than that of BIIB021, suggesting that it is a hydroxylated metabolite. The product ion at m/z 166 obtained from the aglycone (m/z 335) was formed from the pyridine ring moiety, suggesting that the hydroxylation had occurred on this ring. M4 has the same HPLC retention time to that of a reference standard of 5-hydroxymethyl-BIIB021 glucuronide (5-OH 1983 Gluc). All product ions of M4 were consistent with those of 5-OH 1983 Gluc. Therefore, M4 was identified as the glucuronide conjugate of 5-hydroxymethyl-BIIB021.

Metabolite M6 was detected in all samples. It eluted at ca. 33.1 min and produced protonated molecular ions at m/z 301/303. The molecular weight (18 Da lower than BIIB021) and the ratio of isotopic ions 301/303 (1:3) suggest the loss of a chlorine atom and the addition of a hydroxyl group to BIIB021. The product ions at m/z 152/154, 18 Da lower than ion at m/z 170/172 from BIIB021 (Supplemental Figure 3), indicated that de-chlorination and hydroxylation had occurred at the 2-amino-4-chlorine-purine moiety. The product ions at m/z 150 and 120 were the same as those observed for BIIB021. M6 was tentatively identified as a de-chlorinated-hydroxylated metabolite of BIIB021.

Metabolite M7 was detected in all species. It eluted at ca. 35.98 min on HPLC and produced protonated molecular ions at m/z 335/337. With 16 Da higher molecular ion compared to BIIB021, it was proposed as a hydroxylated metabolite. The product ion at m/z 166, 16 Da higher than that of the fragment ion at m/z 150 from the parent suggested that the hydroxylation had occurred at the pyridine ring (Fig. 5A). M7 has the same HPLC retention time to that of a reference standard 5-hydroxymethyl-BIIB021 (CF3785). All product ions of M7 were consistent with those of CF3785. Therefore, M7 was identified as the 5-hydroxymethyl-BIIB021.

Metabolite M10 was detected in all species. It eluted at ca. 40.56 min on HPLC and produced protonated molecular ions at m/z 335/337, 16 Da higher than BIIB021. The product ion at m/z 284, 16 Da higher than that of the fragment ion at m/z 268 from the parent, suggested the addition of one oxygen atom to the purine moiety (Fig. 5B). The product ion at m/z 186, 16 Da higher than that of the fragment ion at m/z 170, also indicated that the hydroxylation had occurred at the 2-amino-4-chlorine-purine moiety. The fragment ions of m/z 120 and 150 were unchanged. M10 has the same HPLC retention time to that of a reference standard of 2-amino-6-chloro-9-((4-methoxy-3,5-dimethylpyridin-2-yl)methyl)-9H-purin-8-ol (CF2483). All product ions of M10 were consistent with those of CF2483. Therefore, M10 was identified as a hydroxylated metabolite, the isomer of M7.

Metabolite M11 and M12 were detected only in the rat hepatocytes. M11 eluted at ca.13.8 min on HPLC and produced protonated molecular ions at m/z 170/172, consistent with ion of 2-amino-4-chlorine-purine moiety. All product ions had isotopic ratios that were consistent with commercial 7-chloro-1H-[1,2,3]triazolo[4,5-d]pyrimidin-5-amine (Supplemental Figure 4). Therefore, M11 was identified as 7-chloro-1H-[1,2,3]triazolo[4,5-d]pyrimidin-5-amine.

M12 eluted at ca. 14.3 min on HPLC and produced a protonated molecular ion at m/z 168 as a non-radiolabel metabolite. The product ion at m/z 150 and m/z 120 were formed from consecutive losses of a water molecule and a methoxyl group (Supplemental Figure 5). Therefore, M12 was tentatively assigned as (4-methoxy-3,5-dimethylpyridin-2-yl)methanol.

Metabolite M13 was detected in rat and dog hepatocyte incubations. It eluted at ca.17.89 min on HPLC and had protonated molecular ions at m/z 493/495. The HRMS of molecular $[M+H]^+$ ion 493.1675 suggests a molecular formula of $C_{20}H_{24}N_6O_9$. The ratio of ions at m/z 493/495 was 1:3 indicating loss of the chlorine atom. The product ions at m/z 317/319 and 299/301 corresponded to the sequential loss of a glucuronic acid moiety (-176 Da) and a water molecule (Supplemental Figure 6). The product ion at m/z 166, 16 Da higher than that of the fragment ion at m/z 150 from the parent, suggested that the addition of an oxygen atom had occurred at the pyridine moiety. M13 was tentatively assigned as the 2-((6-((2-amino-6-hydroxy-9H-purin-9-yl)methyl)-4-methoxy-5-methylpyridin-3-yl)methoxy)-6-(hydroxymethyl)tetrahydro-2H-pyran-3,4,5-triol formed via oxidative dechlorination of the 2-amino-4-amino-chloropurine moiety and hydroxylation followed by glucuronidation on the pyridine moiety.

Metabolite M14 was detected only in dog hepatocytes. It eluted at ca.18.23 min and produced the protonated molecular ions at m/z 576/578. The ratio of isotopic ions 580 ($M+4$) vs 576 was reduced to 0.15: 1, suggesting loss of a chlorine atom. The product ions at m/z 447/449 and 303/305 were formed from loss of the anhydroglutamic acid (-129 Da) and glutamine-alanine-glycine (-273 Da), suggesting that it was a glutathione conjugate (Supplemental Figure 7). MS^3 spectra of ions at m/z 303/305 provided fragments at m/z 270/272 and 136 via loss of an SH and the purine moiety, respectively. The fragment ion at m/z 136, 14 Da lower than that of the fragment ion at m/z 150 from the parent, suggested demethylation at the pyridine ring. HRMS of $[M+H]^+$ at m/z 576.1985 suggests a molecular formula of $C_{23}H_{29}N_9O_7S$. Loss of the GSH ($C_{10}H_{17}N_3O_6S$) from molecular formula gave an ion at m/z 269, which is a typical

product ion of M2 by loss of an HCl molecule. M14 was therefore tentatively assigned as a GSH conjugate of deschloro M2.

Metabolite M15 was detected only in human hepatocytes. It eluted at 21.82 min and produced the protonated molecular ions at m/z 317/319. The 1:3 ratio of isotopic ions at m/z 317/319 suggested loss of a chlorine atom. The product ions at m/z 152/154, 18 Da lower than those of the 2-amino-4-chlorine-purine moiety (Supplemental Figure 8), indicated that oxidative de-chlorination had occurred at this moiety. The product ion at m/z 166, 16 Da higher than that of the fragment ion at m/z 150 from the parent, suggested that hydroxylation had occurred at the pyridine ring. M15 was tentatively assigned as the monohydroxylated M6. The hydroxylation site could not be fully determined by MS data.

Metabolite M16 was detected only in human hepatocytes. It eluted at 22.83 min on HPLC and had protonated molecular ions at m/z 321/323. The product ions at m/z 186/188, 16 Da higher than that of the fragment at m/z 170/172 from the parent (Supplemental Figure 9), suggested that the hydroxylation had occurred at the 2-amino-4-chlorine-purine moiety. The product ions at m/z 136 and 108 were formed from the pyridine ring moiety by subsequent losses of the 2-amino-4-chlorine-purine and CO moieties (-28 Da). The ion at m/z 136, 14 Da lower than ion at m/z 150 of parent molecule, suggested the loss of a methyl group from the pyridine ring. M16 was tentatively assigned as a demethylated M10 or monohydroxylated M2.

Metabolite M17 was detected in hepatocytes of all species. It eluted at 25.06 min and had the protonated molecular ions at m/z 606/608. The ratio of isotopic ions 610 (M+4) vs 606 was reduced to 0.15: 1, suggesting loss of the chlorine. The product ions at

m/z 477/479 corresponded to loss of the anhydroglutamic acid (-129 Da). The product ions at m/z 333/335 were due to cleavage of the S-CH₂ bond leading to a neutral loss of 273 Da (Supplemental Figure 10). HRMS of [M+H]⁺ ion 606.2085 suggests a molecular formula of C₂₄H₃₁N₉O₈S. Loss of GSH (C₁₀H₁₇N₃O₆S) from molecular formula gave the same ion at m/z 299, which is a typical product ion of M7 by loss of an HCl molecule. M17 was therefore tentatively assigned as the GSH conjugate of dechlorinated M7. The location of hydroxylation could not be determined by MS data.

Metabolite M18 was detected in rat and dog hepatocytes. It eluted at ca.34.6 min and had protonated molecular ions at m/z 590/592/594. The ratio of isotopic ions 594 (M+4) vs 590 was reduced to 0.20: 1, suggesting loss of a chlorine atom. The product ion at m/z 461/463 corresponded to the loss of the anhydroglutamic acid (-129 Da, Fig. 6A). The product ions at m/z 317/319 were due to cleavage of the S-CH₂ bond leading to a neutral loss of 273 Da. The product ions at m/z 150 and 120 in MS³ spectrum (Fig. 6B) were the same as those observed in BIIB021. HRMS of [M+H]⁺ ion 590.2130 suggests a molecular formula of C₂₄H₃₁N₉O₇S. Loss of GSH (C₁₀H₁₇N₃O₆S) from the molecular ion gave the same ion at m/z 283, which is a typical product ion of BIIB021 by loss of an HCl molecule. M18 was tentatively identified as the GSH conjugate of deschloro- BIIB021.

Metabolism by cDNA-Expressed CYP450s and Monoclonal Antibody Inhibition

Human recombinant CYP2C19, CYP2C9, and CYP3A4 isoforms showed catalytic activity of BIIB021 metabolite formation (Fig. 7). [¹⁴C]BIIB021 was completely metabolized by CYP2C19. Average 5% and 89% radioactivity presented as M2 and M7, respectively. With human recombinant CYP3A4, 70% radioactivity remained as parent.

Approximately 5% and 21% radioactivity presented as M2 and M7, respectively. Human CYP2C9 had the lowest catalytic activity and only 2.5% radioactivity was detected as metabolite M7. The rest of radioactivity remained as parent. It appeared that CYP2C19 and CYP3A4 were main liver microsomal enzymes responsible for the formation of hydroxy (M7) and desmethyl- (M2) metabolites.

To further confirm the primary CYP enzymes involved in BIIB021 metabolism, several monoclonal antibodies of CYP enzymes were added into human liver microsomal incubations (Fig. 8A). With anti-CYP2C19 or anti-CYP3A4, maximum inhibition of M7 formation was achieved at 75.6% or 34%, respectively (Fig. 8B). Other monoclonal antibodies such as CYP1A2, CYP2A6, CYP2B6, CYP2D6, and CYP2E1 did not show significant inhibition of M7 formation (Fig. 8A). The inhibitory effect of monoclonal antibody on M2 formation were not observed significantly in this experiment.

Metabolism by Cytosolic Enzymes

Metabolite M10 was detected as a non-NADPH/NAD dependent metabolite in human cytosolic incubation. To determine the major enzymes involved in the formation of M10, specific inhibitors of xanthine oxidase and AO were added into cytosolic incubation. As shown in Fig.9, M10 formation was not impacted by addition of xanthine oxidase inhibitor, allopurinol (Clarke *et al.*, 1995; Rashidi *et al.*, 2007). In contrast, M10 formation was significantly inhibited by AO inhibitors, isovanillin, menadione, and raloxifene (Obach, 2004; Rashidi *et al.*, 2007). The results suggested that the formation of M10 is probably catalyzed by AO.

Glutathione conjugate metabolite M18 was formed both chemically and enzymatically catalyzed by GST. After [¹⁴C]BIIB021 was incubated in GSH fortified

phosphate buffer and human liver microsomes, approximately 20% total radioactivity was identified as M18 in both incubations (Fig. 10), suggesting a non-enzymatic GSH substitution reaction. When incubated with GSH fortified human liver cytosol, ~55% [¹⁴C]BIIB021 was converted to M18. After GST inhibitor ethacrynic acid was added in the cytosolic incubation, the amount of M18 was reduced to 20%, which was equivalent to the extent of M18 formation observed in the buffer. This result suggested that M18 formation was predominantly catalyzed by cytosolic GST in the liver. Similar chlorine displacement by water (M6) was also observed but the percentage of M6 remained 1~3% across all incubations (data not shown).

Discussion

The *in vitro* metabolism of BIIB021 in liver microsomes and hepatocytes of rats, dogs, and humans has been elucidated to support preclinical safety and clinical studies. Rats and Dogs were chosen in this study because they are species used for preclinical safety assessments. BIIB021 is extensively metabolized in both liver microsomes and hepatocytes and a total of 13 metabolites were identified by LC-MS/MS. The major metabolites were similar in all species (Table 3 and Fig. 11). However, several additional metabolites were identified in the rat hepatocytes. The primary major metabolic pathways were due to hydroxylation of the methyl group, *O*-demethylation, *N*-dealkylation of the methoxy-dimethylpyridine moiety, oxygenation of the purine and direct displacement of the chlorine with GSH or water (Fig. 11). The other metabolites were due to combination of these primary pathways. Most of these metabolites do not exhibit pharmacological activity except M7 and M10, which were 10 and 5 fold less potent than the parent BIIB021, respectively.

After incubation of [¹⁴C]BIIB021 with liver microsomes fortified with NADPH, mono-hydroxylation and *O*-demethylation at the methoxy-dimethylpyridine moiety were identified as the major metabolic pathways in three species and yielded metabolites M7 and M2, respectively. Consistent with LM incubations, mono-hydroxylation at the methoxy-dimethylpyridine moiety was also observed as a major metabolic pathway in hepatocytes. Majority of M7 in dog hepatocytes was further metabolized to form a glucuronide conjugate M4. *O*-Demethylation (M2) was also a major metabolic pathway in rat and dog. Qualitative identification using cDNA-expressed CYP450s suggested that monohydroxylation and demethylation are mainly catalyzed by CYP2C19 and CYP3A4.

Although CYP2C19 showed higher catalytic activity of monohydroxylation, the amount of CYP2C19 in human liver is less than 1% of the total CYP450s (Inoue *et al.*, 1997). The contribution to monohydroxylation of BIIB021 could be balanced by both CYP2C19 and dominant CYP450 enzyme CYP3A4. In the CYP antibody inhibition study in human liver microsomes, it appeared that CYP2C19 and CYP3A4 were responsible for 65~75% and 25~35% formation of M7. Similarly, oxidative *O*-demethylation is expected to be mainly catalyzed by human CYP3A4 when approximately equal amount of M2 formation was observed by using equal molarity of human recombinant CYP2C19 and CYP3A4.

The oxidative *N*-dealkylation of the 4-methoxy-3,5-dimethylpyridine moiety (M11 and M12) was unique metabolic pathway in the rat. It was not observed either in human or dog. Non-enzymatic oxidative dechlorination of BIIB021 (M6) and its metabolites (M13 and M15) observed during the incubation was indicative of the instability of BIIB021 chlorine moiety in aqueous solution. M13 and M15 were probably formed from non-enzymatic oxidative dechlorination of M4 and M7, respectively.

In this study, several GSH adducts formed via the displacement of the chlorine on the amino-chloropurine moiety were observed in hepatocytes incubations. M18 was formed via direct GSH substitution of chlorine on purine moiety. The substitution was predominantly catalyzed by cytosolic GST. The GSH substitution on 2-chloropyridines has been reported but it is catalyzed by microsomal GST (Inoue *et al.*, 2009). M14 and M17 were formed probably from GSH substitution of M2 and M7, respectively. The evidence of GSH substitution could suggest potential covalent binding of BIIB021 or its metabolites to endogenous proteins (Nakayama *et al.*, 2011). After incubation of [¹⁴C]BIIB021 with hepatocytes, the recovery of radioactivity reached above 85%,

indicating the covalent protein binding potential may be lower than 15% and GSH may play an important role to protect undesired covalent binding of endogenous proteins. Since this substitution of chlorine with GSH occurred both chemically and enzymatically catalyzed by cytosolic GST, any undesired toxicity could be assessed in rat and dog toxicological studies. The GSH substitution pathway was also confirmed during metabolic profiling studies *in vivo* and mercapturic acid of substituted BIIB021 was detected in urine (Xu *et al.*, 2010).

Monohydroxylation on the purine moiety (M10) was identified as a minor metabolic pathway in liver microsomes and hepatocytes. Interestingly, M10 formation was found NADPH and NAD⁺ independent and the hydroxylation occurred on the hetero-aromatic purine moiety. These observations suggested that M10 formation was probably catalyzed by a cytosolic enzyme such as AO, xanthine dehydrogenase, and xanthine oxidase. The NAD⁺ independence of reaction excluded the possibility of a xanthine dehydrogenase. The further inhibition studies demonstrated that the formation of M10 was completely inhibited by several AO inhibitors but not by a xanthine oxidase inhibitor, allopurinol. Therefore, AO appeared to catalyze the formation of M10. It is reported that AO expression levels vary markedly across species with the high activity in monkey and human, and relatively lower activity in rat and mouse, and the lowest activity in dogs and birds (Sahi *et al.*, 2008). The trace amount of M10 formation in LM incubation might attribute to incomplete isolated cytosolic AO. The trace amount of M10 was also observed in dog LM and hepatocyte although dog is recognized devoid of AO activity in the liver (Beedham *et al.*, 1987; Terao *et al.*, 2006). The trace amount of M10 was also identified as a minor metabolite in dog plasma and urine when administered of

BIIB021 orally in dog (Xu *et al.*, 2010). The reason is not clear. It might indicate that dog maintains minimal AO activity or another enzyme in dog catalyzes M10 formation. In addition to M10, the formation of M16, which was identified only in human hepatocyte incubation, was also catalyzed by AO. It was formed by combination of purine hydroxylation and *O*-demethylation via M10 or M2. The combined radioactivity of M10 and M16 in hepatocyte incubation was 3.6% in human, 0.4% in dog, and 0.4% in the rat. Higher turnover on AO catalyzed biotransformation of BIIB021 in human than in dog or rat was consistent with reported species variability of AO expressing level. Meanwhile, AO is not only expressed in liver, also predominantly expressed in the lung, kidney, and other tissues (Kitamura *et al.*, 2006). The inter-individual variability of AO activity was also observed high in the liver (Lake *et al.*, 2002; Sugihara *et al.*, 1997). Hence, contribution of AO to BIIB021 metabolism in hepatocytes only may underestimate its actual effect in clinic pharmacokinetic and metabolism. *In vivo* and *in vitro* metabolism of BIIB021 in dogs and rats might also underestimate AO contribution in humans.

The U.S. Food and Drug Administration (FDA, 2008) and International Conference on Harmonization (Guidance on Non-Clinical Safety Studies for the Conduct of Human Clinical Trials and Marketing Authorization for Pharmaceuticals, 2009) have recently issued a formal guidance on the safety testing of drug metabolites. Based on current C14-labeled *in vitro* metabolism study, majority of identified human metabolites will be covered by preclinical species. Mono-hydroxylated metabolite M7 and *O*-demethylated metabolite M2 were also predominant in animal species. However, formation of metabolites via AO pathway such as M10 and M16 is relatively low or

negligible in rat and dog. In order to have safety coverage of M10 in preclinical species, higher dose treatment in toxicology studies and large safety window of BIIB021 are required.

In summary, the results of this study provide the first analysis of characterization of metabolites of BIIB021 in liver microsomes and hepatocytes from rat, dog and human. Based on the structures of metabolites, four major metabolic pathways involving two hydroxylation, non-enzymatic/enzymatic water/GSH substitution, and *O*-demethylation were observed in all species. The oxidative *N*-dealkylation pathway was unique in the rat. On the basis of these data, it is expected that BIIB021 will be biotransformed in human by multiple pathways. Two monohydroxylation pathways were catalyzed by two polymorphic enzymes CYP2C19 (Shon *et al.*, 2002) and AO. It could contribute to inter-individual metabolite concentration of M7 or M10. The results of this study will aid in the identification of metabolites of BIIB021 in humans *in vivo* and the evaluation of potential drug-drug interaction in clinic.

Acknowledgments

We would like to thank Dr. Ryan Van de Water for synthesizing [^{14}C] BIIB021, and Dr. Marco Biomonte, Kevin Hong, and Jiandong Shi for providing synthetic standards of metabolites.

Authorship Contributions

Participated in research design: Lin Xu, Chandra Prakash.

Conducted experiments: Caroline Woodward, Samina Khan

Contributed new reagents or analytic tools: Caroline Woodward, Samina Khan, Chandra Prakash

Performed data analysis: Lin Xu, Caroline Woodward, Samina Khan, Chandra Prakash

Wrote or contributed to the writing of the manuscript: Lin Xu, Caroline Woodward, Chandra Prakash

References

Baillie TA, Cayen MN, Fouda H, Gerson RJ, Green JD, Grossman SJ, *et al.* (2002). Drug metabolites in safety testing. *Toxicol Appl Pharmacol* **182**(3): 188-196.

Baranczewski P, Stanczak A, Kautiainen A, Sandin P, Edlund PO (2006). Introduction to early in vitro identification of metabolites of new chemical entities in drug discovery and development. *Pharmacol Rep* **58**(3): 341-352.

Beedham C, Bruce SE, Critchley DJ, al-Tayib Y, Rance DJ (1987). Species variation in hepatic aldehyde oxidase activity. *Eur J Drug Metab Pharmacokinet* **12**(4): 307-310.

Biamonte MA, Van de Water R, Arndt JW, Scannevin RH, Perret D, Lee WC (2010). Heat shock protein 90: inhibitors in clinical trials. *J Med Chem* **53**(1): 3-17.

Clarke SE, Harrell AW, Chenery RJ (1995). Role of aldehyde oxidase in the in vitro conversion of famciclovir to penciclovir in human liver. *Drug Metab Dispos* **23**(2): 251-254.

Dalvie D, Obach RS, Kang P, Prakash C, Loi CM, Hurst S, *et al.* (2009). Assessment of three human in vitro systems in the generation of major human excretory and circulating metabolites. *Chem Res Toxicol* **22**(2): 357-368.

FDA (2008). Guidance for Industry: Safety Testing of Drug Metabolites:
<http://www.fda.gov/cder/guidance/6897fnl.pdf>.

Inoue K, Ohe T, Mori K, Sagara T, Ishii Y, Chiba M (2009). Aromatic substitution reaction of 2-chloropyridines catalyzed by microsomal glutathione S-transferase 1. *Drug Metab Dispos* **37**(9): 1797-1800.

Inoue K, Yamazaki H, Imiya K, Akasaka S, Guengerich FP, Shimada T (1997). Relationship between CYP2C9 and 2C19 genotypes and tolbutamide methyl hydroxylation and S-mephenytoin 4'-hydroxylation activities in livers of Japanese and Caucasian populations. *Pharmacogenetics* **7**(2): 103-113.

Kasibhatla SR, Boehm MF, Hong KD, Biamonte MA, Shi J, Le BJ-y, *et al.* (2005). Preparation of novel heterocyclic compounds such as aminopurines, aminopyrrolopyrimidines, aminopyrazolopyrimidines and aminotriazolopyrimidines as HSP90-inhibitors, p 506 pp.: Conforma Therapeutics Corporation, USA .

Kasibhatla SR, Hong K, Biamonte MA, Busch DJ, Karjian PL, Sensintaffar JL, *et al.* (2007). Rationally designed high-affinity 2-amino-6-halopurine heat shock protein 90 inhibitors that exhibit potent antitumor activity. *J Med Chem* **50**(12): 2767-2778.

Kitamura S, Sugihara K, Ohta S (2006). Drug-metabolizing ability of molybdenum hydroxylases. *Drug Metab Pharmacokinet* **21**(2): 83-98.

Lake BG, Ball SE, Kao J, Renwick AB, Price RJ, Scatina JA (2002). Metabolism of zaleplon by human liver: evidence for involvement of aldehyde oxidase. *Xenobiotica* **32**(10): 835-847.

Lundgren K, Zhang H, Brekken J, Huser N, Powell RE, Timple N, *et al.* (2009). BIIB021, an orally available, fully synthetic small-molecule inhibitor of the heat shock protein Hsp90. *Mol Cancer Ther* **8**(4): 921-929.

Nakayama S, Takakusa H, Watanabe A, Miyaji Y, Suzuki W, Sugiyama D, *et al.* (2011). Combination of GSH Trapping and Time-Dependent Inhibition Assays as a Predictive Method of Drugs Generating Highly Reactive Metabolites. *Drug Metab Dispos* **39**(7): 1247-1254.

Obach RS (2004). Potent inhibition of human liver aldehyde oxidase by raloxifene. *Drug Metab Dispos* **32**(1): 89-97.

Pearl LH, Prodromou C (2006). Structure and mechanism of the Hsp90 molecular chaperone machinery. *Annu Rev Biochem* **75**: 271-294.

Rashidi MR, Beedham C, Smith JS, Davaran S (2007). In vitro study of 6-mercaptopurine oxidation catalysed by aldehyde oxidase and xanthine oxidase. *Drug Metab Pharmacokinet* **22**(4): 299-306.

Sahi J, Khan KK, Black CB (2008). Aldehyde oxidase activity and inhibition in hepatocytes and cytosolic fractions from mouse, rat, monkey and human. *Drug Metab Lett* **2**(3): 176-183.

Shon JH, Yoon YR, Kim KA, Lim YC, Lee KJ, Park JY, *et al.* (2002). Effects of CYP2C19 and CYP2C9 genetic polymorphisms on the disposition of and blood glucose lowering response to tolbutamide in humans. *Pharmacogenetics* **12**(2): 111-119.

Soo ET, Yip GW, Lwin ZM, Kumar SD, Bay BH (2008). Heat shock proteins as novel therapeutic targets in cancer. *In Vivo* **22**(3): 311-315.

Sugihara K, Kitamura S, Tatsumi K, Asahara T, Dohi K (1997). Differences in aldehyde oxidase activity in cytosolic preparations of human and monkey liver. *Biochem Mol Biol Int* **41**(6): 1153-1160.

Terao M, Kurosaki M, Barzago MM, Varasano E, Boldetti A, Bastone A, *et al.* (2006). Avian and canine aldehyde oxidases. Novel insights into the biology and evolution of molybdo-flavoenzymes. *J Biol Chem* **281**(28): 19748-19761.

Xu L, Galluppi J, Klunk LJ, Prakash C (2010). Metabolism and Excretion of a Hsp90 Inhibitor, BIIB021, in Rats and Dogs Following Oral Administration of a Single Dose of [¹⁴C]BIIB021. In: *The AAPS Journal*.

Zhang H, Neely L, Lundgren K, Yang YC, Lough R, Timple N, *et al.* (2010). BIIB021, a synthetic Hsp90 inhibitor, has broad application against tumors with acquired multidrug resistance. *Int J Cancer* **126**(5): 1226-1234.

Footnotes

Send reprint requests to: Lin Xu, Drug Metabolism and Preclinical Safety, Biogen
Idec, Cambridge, MA, 02142; telephone: 617-914-7191; fax: 617-679-3463;
email:lin.xu@biogenidec.com

Figures

- FIG 1. Structure of BIIB021. The position of carbon-14 label is indicated with *.
- FIG 2. LC radio-chromatograms of [^{14}C]BIIB021 metabolites with (A) HLM control without NADPH; (B) HLM fortified with NADPH; (C) DLM fortified with NADPH, (D) RLM fortified with NADPH.
- FIG 3. LC radio-chromatograms of [^{14}C]BIIB021 and metabolites with (A) Krebs buffer as control; (B) human; (C) dog; and (D) rat hepatocytes.
- FIG 4. CID product ion spectra of monoisotopic molecular ions 319 (A, ^{35}Cl), 321 (B, ^{37}Cl), and 323 (C, ^{35}Cl , ^{14}C) of [^{14}C]BIIB021.
- FIG 5. CID product ion spectra of M7 (A) and M10 (B)
- FIG 6. CID product spectrum of M18 (A) and MS^3 of product ion 317 (B).
- FIG 7. Formation of M7 (A) and M2 (B) metabolites by cDNA-expressed human P450s
- FIG 8. Inhibition of M7 formation relative to control by (A) monoclonal CYP antibodies (15 μL) and (B) different concentration of CYP2C19 and CYP3A4 antibodies in human liver microsomal incubations with [^{14}C]BIIB021.
- FIG 9. Effect of allopurinol, isovanillin, menadione, and raloxifene on the formation M10 in human liver cytosolic incubation.
- FIG 10. Percentage of M18 formation in the phosphate buffer (A), phosphate buffer with GSH (B), human liver microsomes with GSH (C), human liver cytosols with GSH (D), and human liver cytosols with GSH and ethacrynic acid (E).
- FIG 11. Proposed metabolic pathways of BIIB021 *in vitro*

Table 1. Percentage of Identified Metabolites in Liver Microsomes

Metabolite	Human		Dog		Rat	
	(-) NADPH	(+)NADPH	(-) NADPH	(+)NADPH	(-) NADPH	(+)NADPH
	<i>% Radioactivity</i>					
M2		3.6		9.5		4.5
M6	0.9	0.5	1.07	0.5	0.5	0.6
M7		42.2		36.2		53.2
M10		0.5		0.3		1.3
M11/M12						6.9
BIIB021	99.1	54.1	98.93	54.2	99.5	34.1

(+) Incubated with NADPH (-) Incubated without NADPH

Table 2. Percentage of Identified Metabolites in Hepatocytes

Metabolite	Krebbs buffer	Human	Dog	Rat
<i>% Radioactivity</i>				
M2		0.5	25.5	8.7
M4			44.8	10.2
M6	3.5	4.4	1.0	0.3
M7		49.0	3.0	37.5
M10		1.7	0.4	0.4
M11				11.1
M13			2.0	4.4
M14			7.0	
M15		3.4		
M16		1.9		
M17		1.8	3.0	9.1
M18			9.0	13.1
BIIB021	96.5	38	0.8	5.2

Table 3. Assignment and Proposed Structures of Metabolites of [¹⁴C]BIIB021

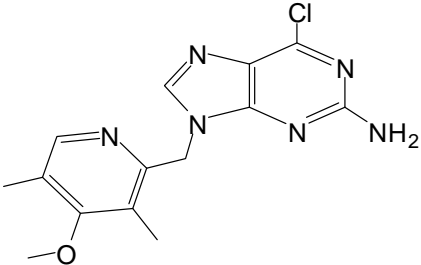
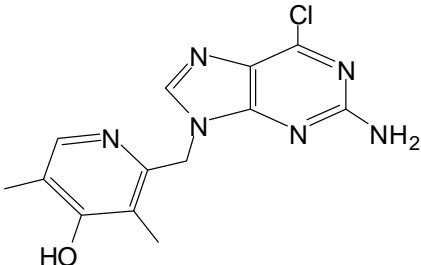
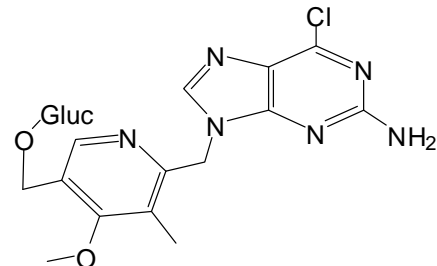
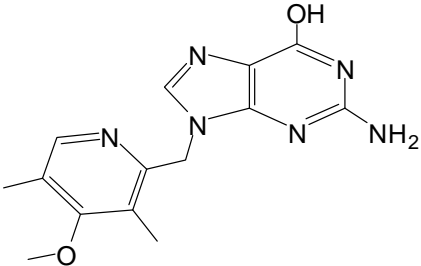
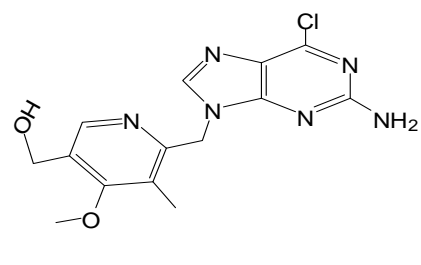
Assignment	¹² C-Mass [M+H] ⁺ m/z HRMS	Proposed Structure ^a	Biotransformation	Major fragments	Rt (min)
BIIB021	319.1070			283, 268, 150, 120	47.89
M2	305.0914		demethylation	269, 170, 136	23.74
M4	511.1338		Hydroxylation and glucuronidation	335, 166	27.23
M6	301.1405		Oxidative dechlorination	152, 150, 120	33.1
M7	335.1016		hydroxylation	166	35.98

Table 3. (continued) Assignment and Proposed Structures of Metabolites of [¹⁴C]BIIB021

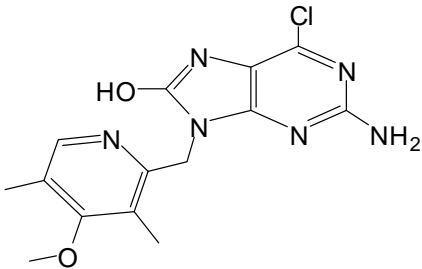
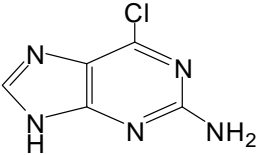
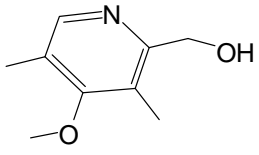
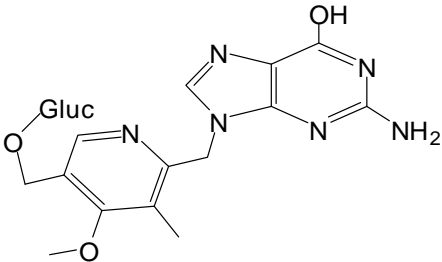
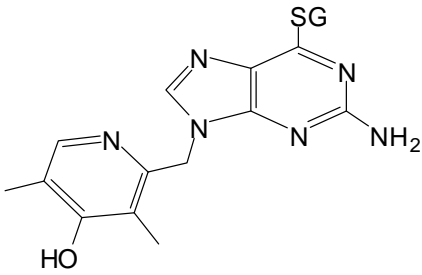
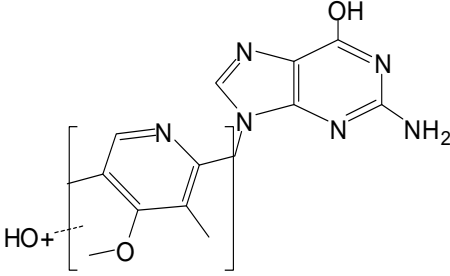
Assignment	¹² C-Mass [M+H] ⁺ m/z HRMS	Proposed Structure	Biotransformation	Major fragments	Rt (min)
M10	335.1017		hydroxylation	284, 186, 150, 120	40.56
M11	170.0232		N-dealkylation	170	13.8
M12	168.1024		Oxidative Dealkylation	150, 120	14.3
M13	493.1674		Oxidative dechlorination and glucuronidation	317, 299, 166	17.89
M14	576.1977		Demethylation and glutathione displacement of chlorine	447, 303, 270, 136	18.23
M15	317.1354		Hydroxylation and oxidative dechlorination	166, 152	21.82

Table 3. (continued) Assignment and Proposed Structures of Metabolites of [¹⁴C]BIIB021

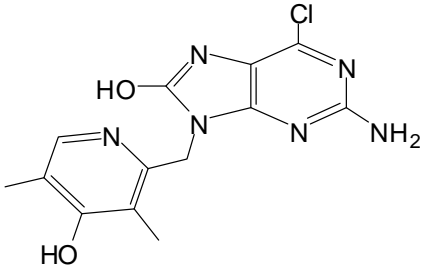
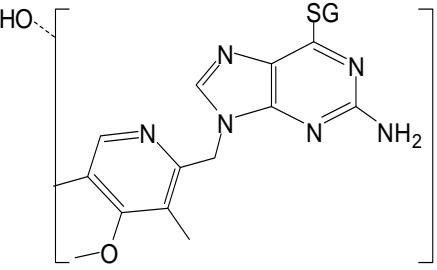
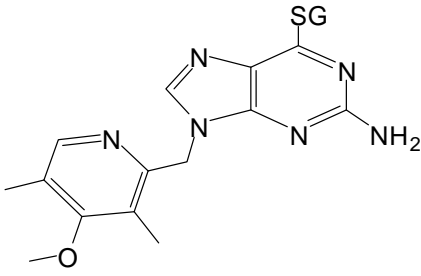
Assignment	¹² C-Mass [M+H] ⁺ m/z HRMS	Proposed Structure	Biotransformation	Major fragments	Rt (min)
M16	321.0870		Demethylation and hydroxylation	186, 136, 108	22.83
M17	606.2085		Hydroxylation and glutathione displacement of chlorine	477, 333	25.06
M18	590.2131		Glutathione displacement of chlorine	461, 317, 150, 120	34.6

Figure 1

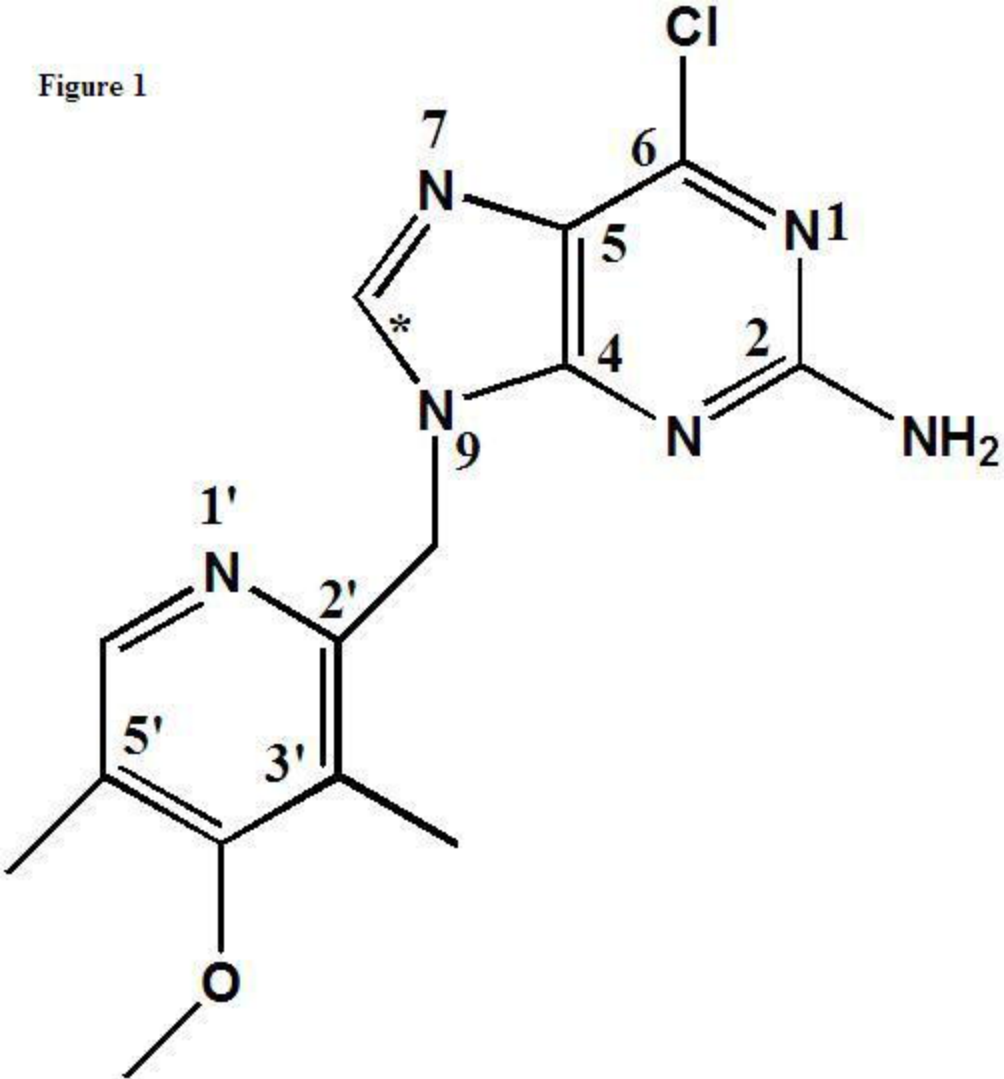


Figure 2

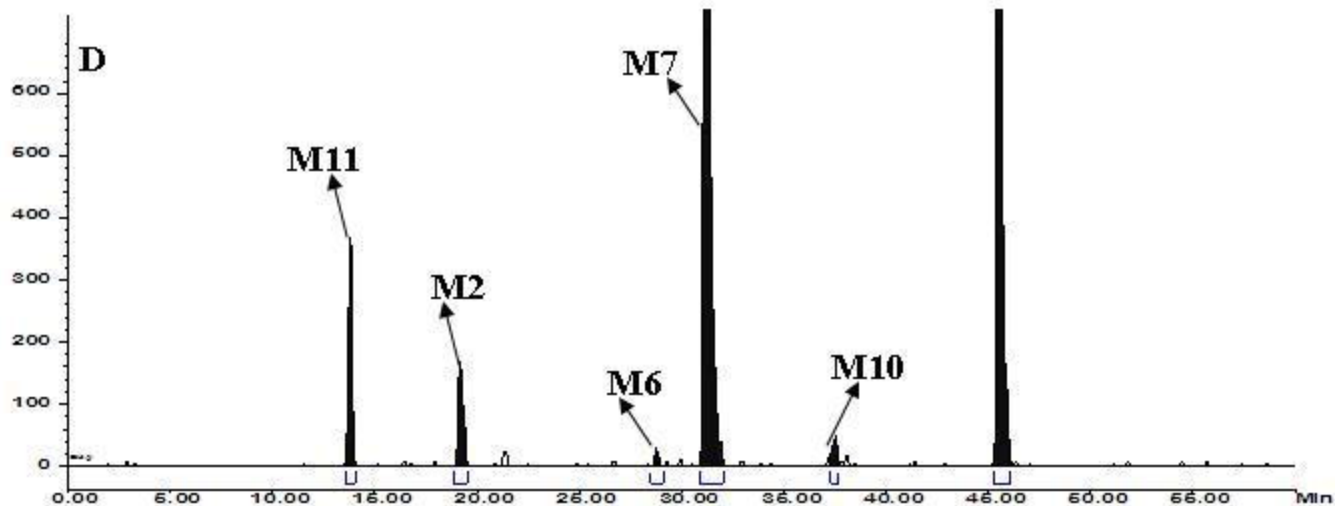
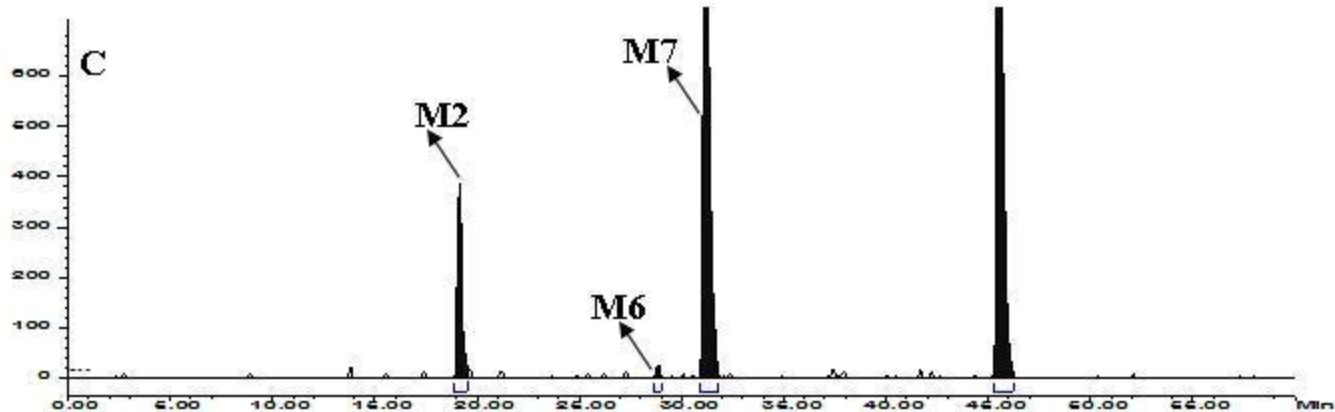
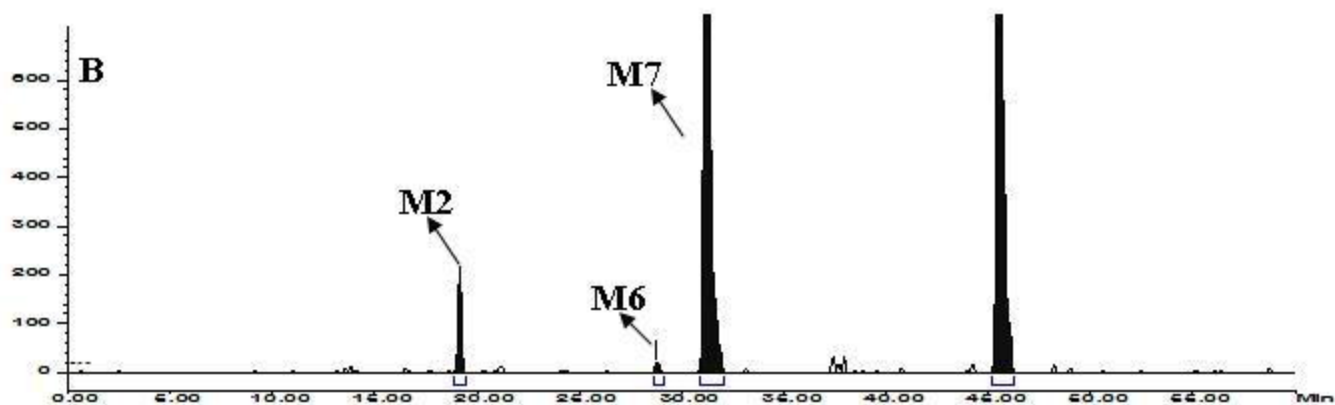
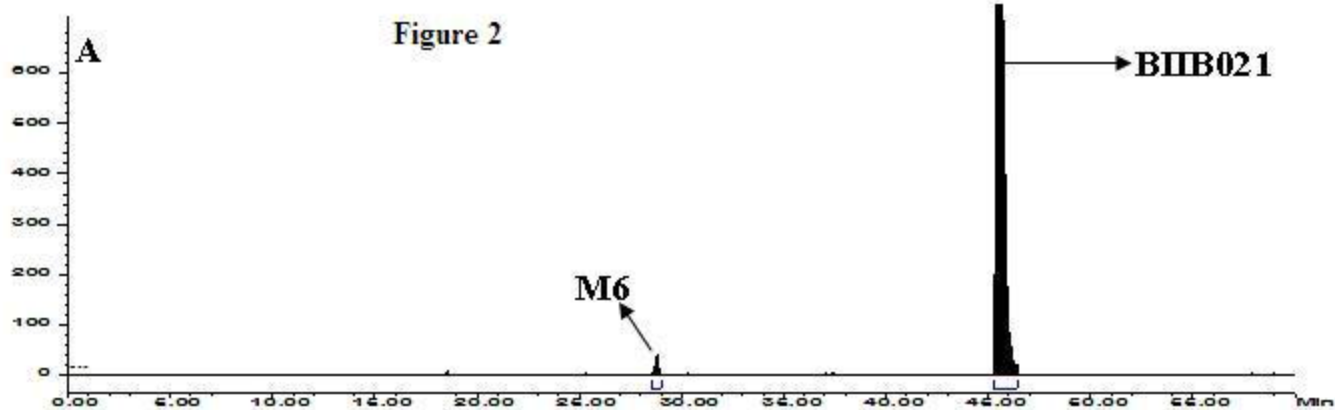


Figure 3

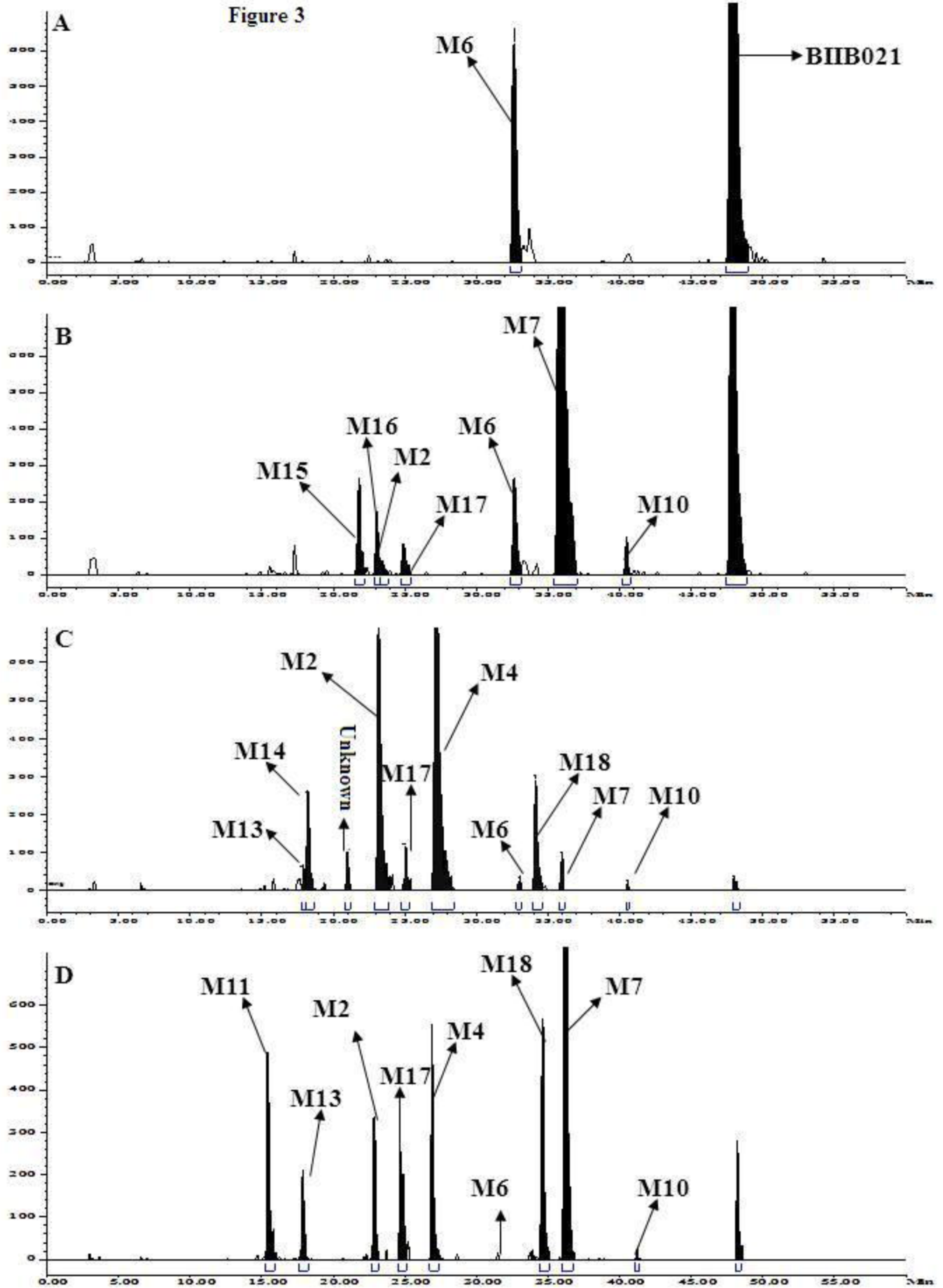


Figure 4

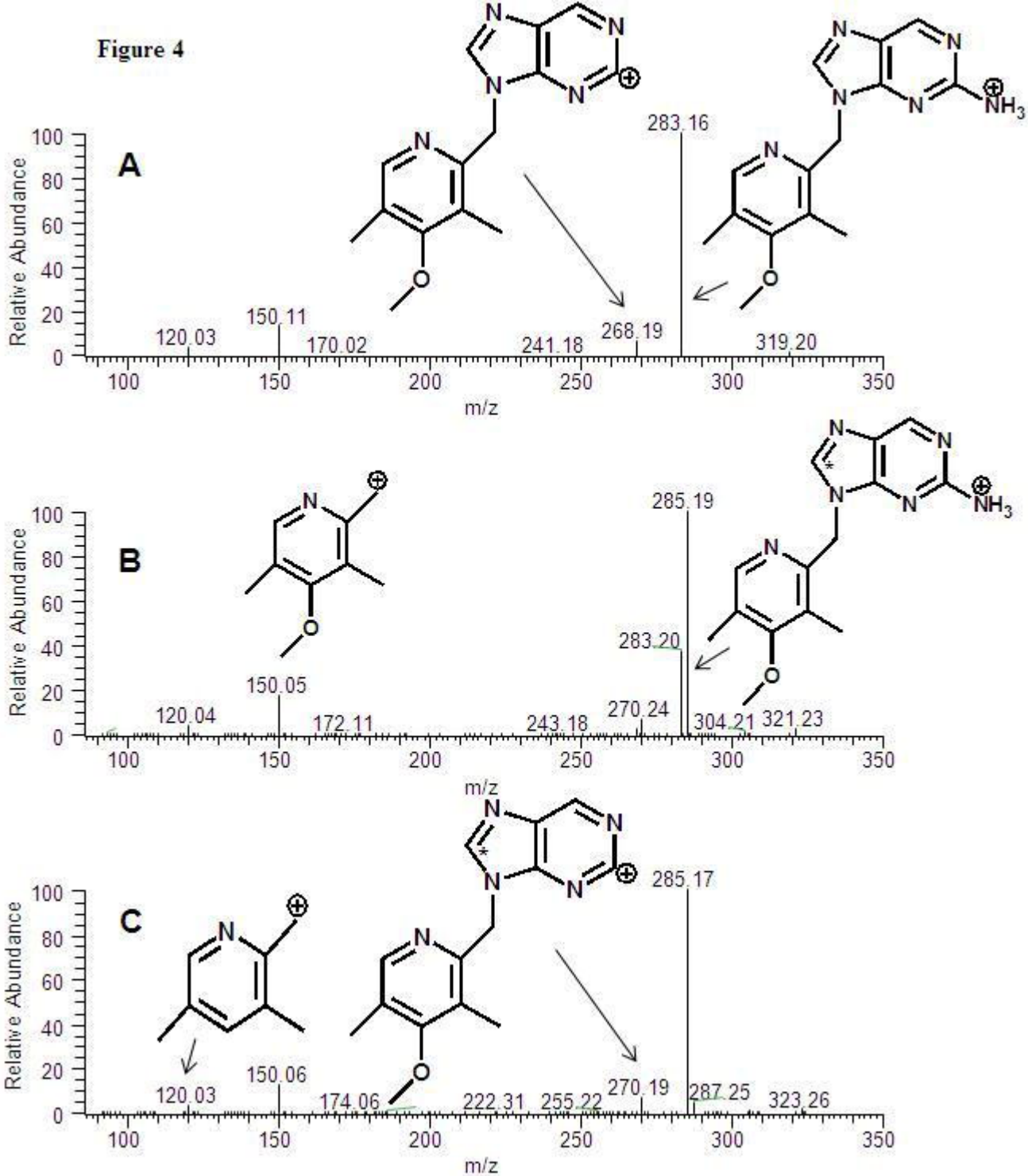


Figure 5

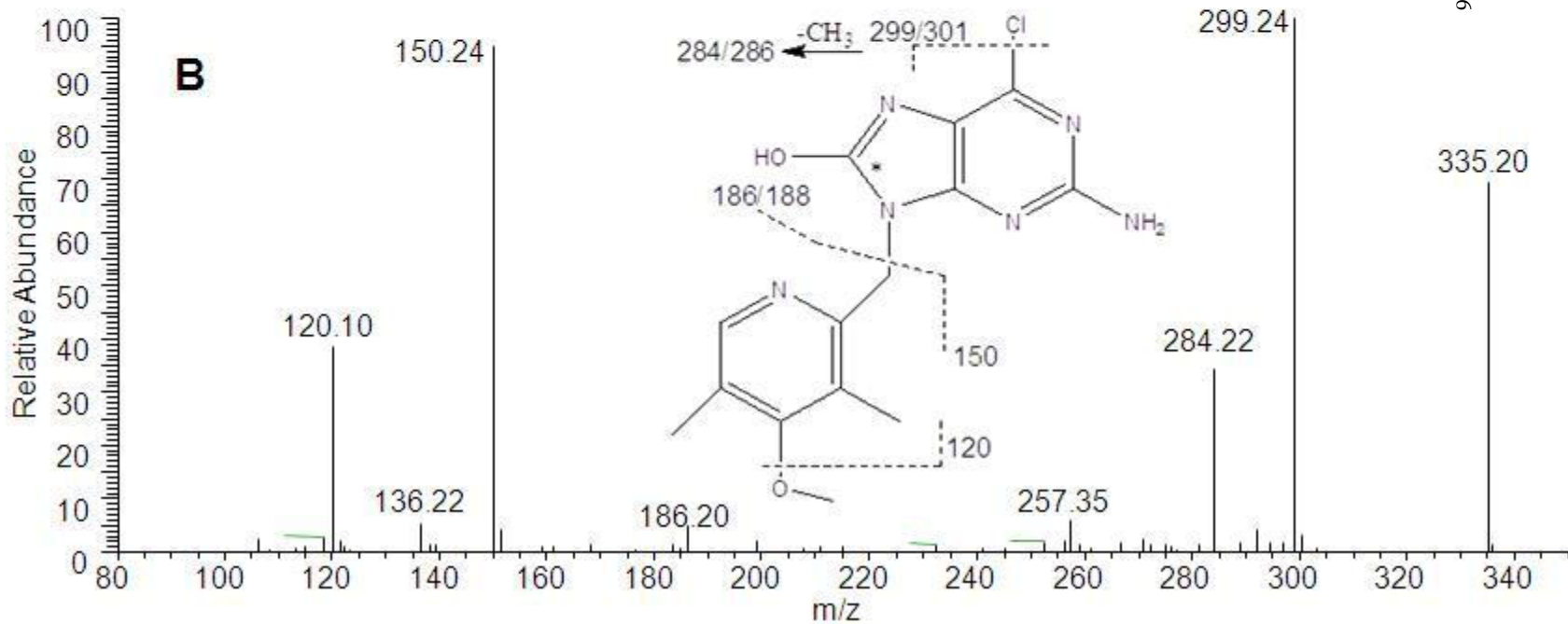
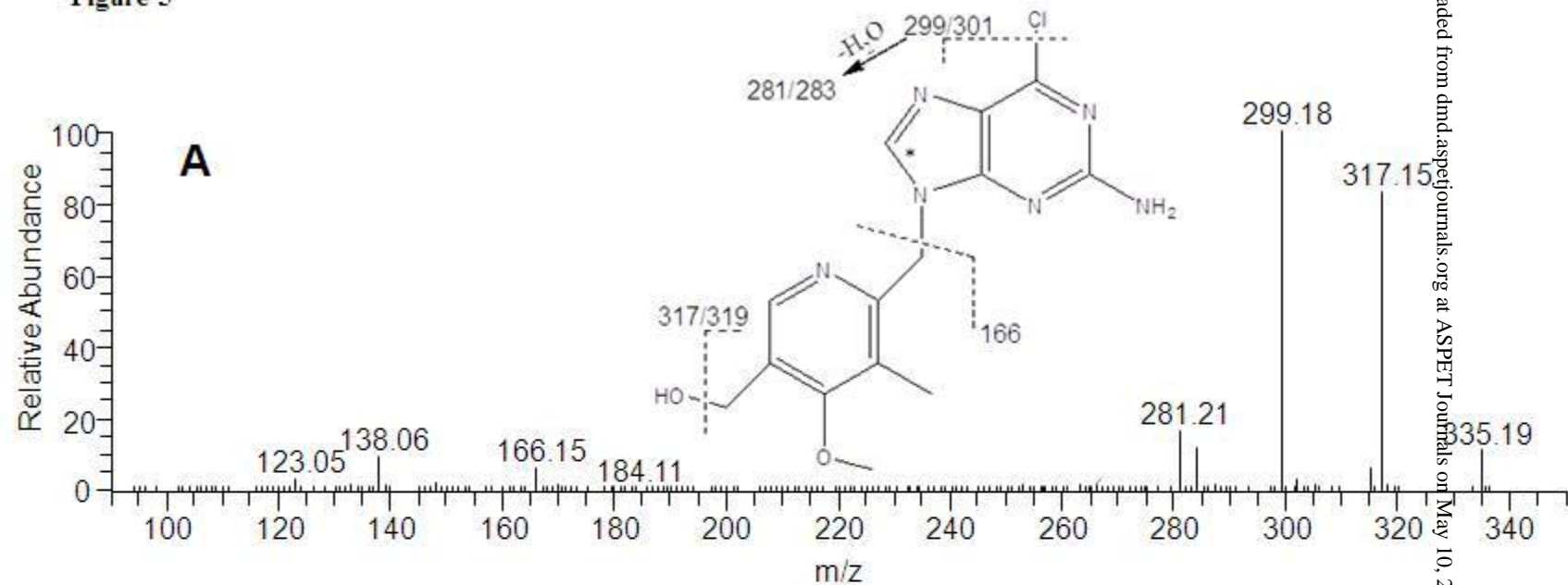


Figure 6

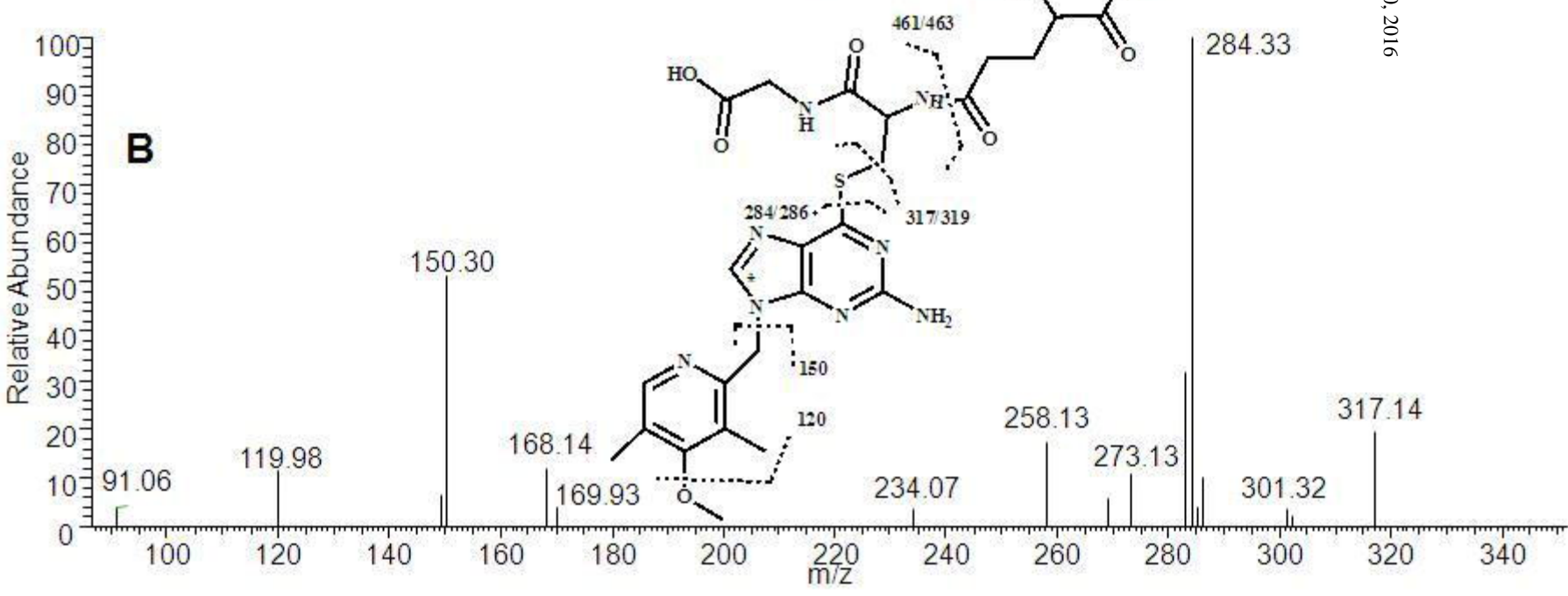
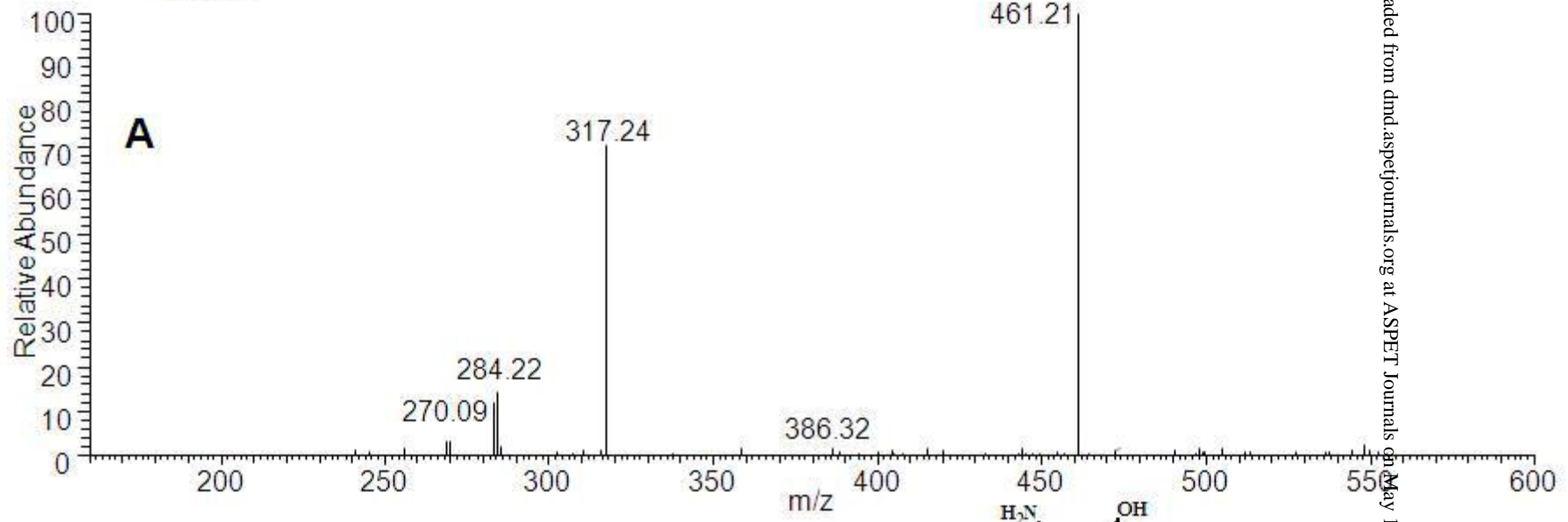


Figure 7

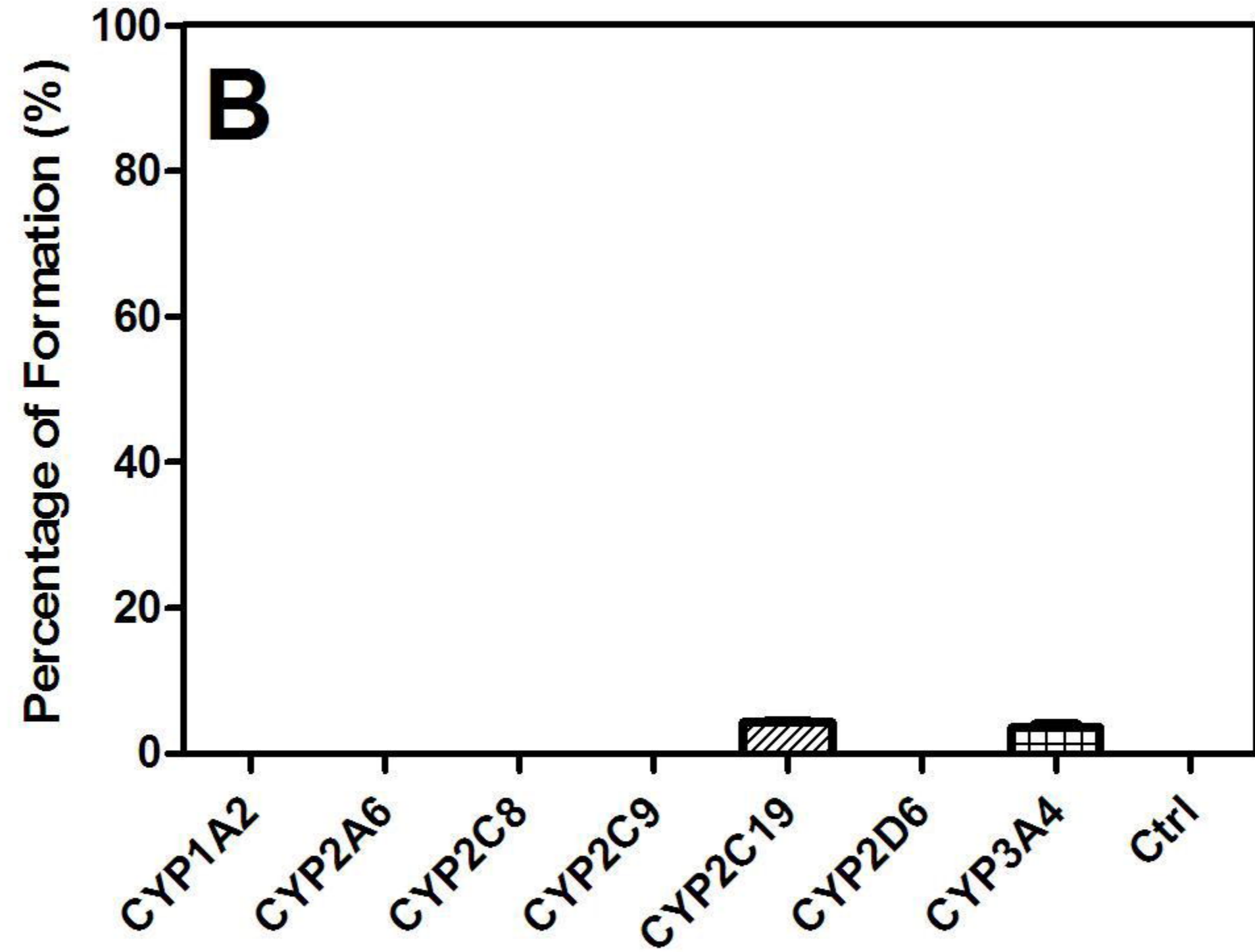
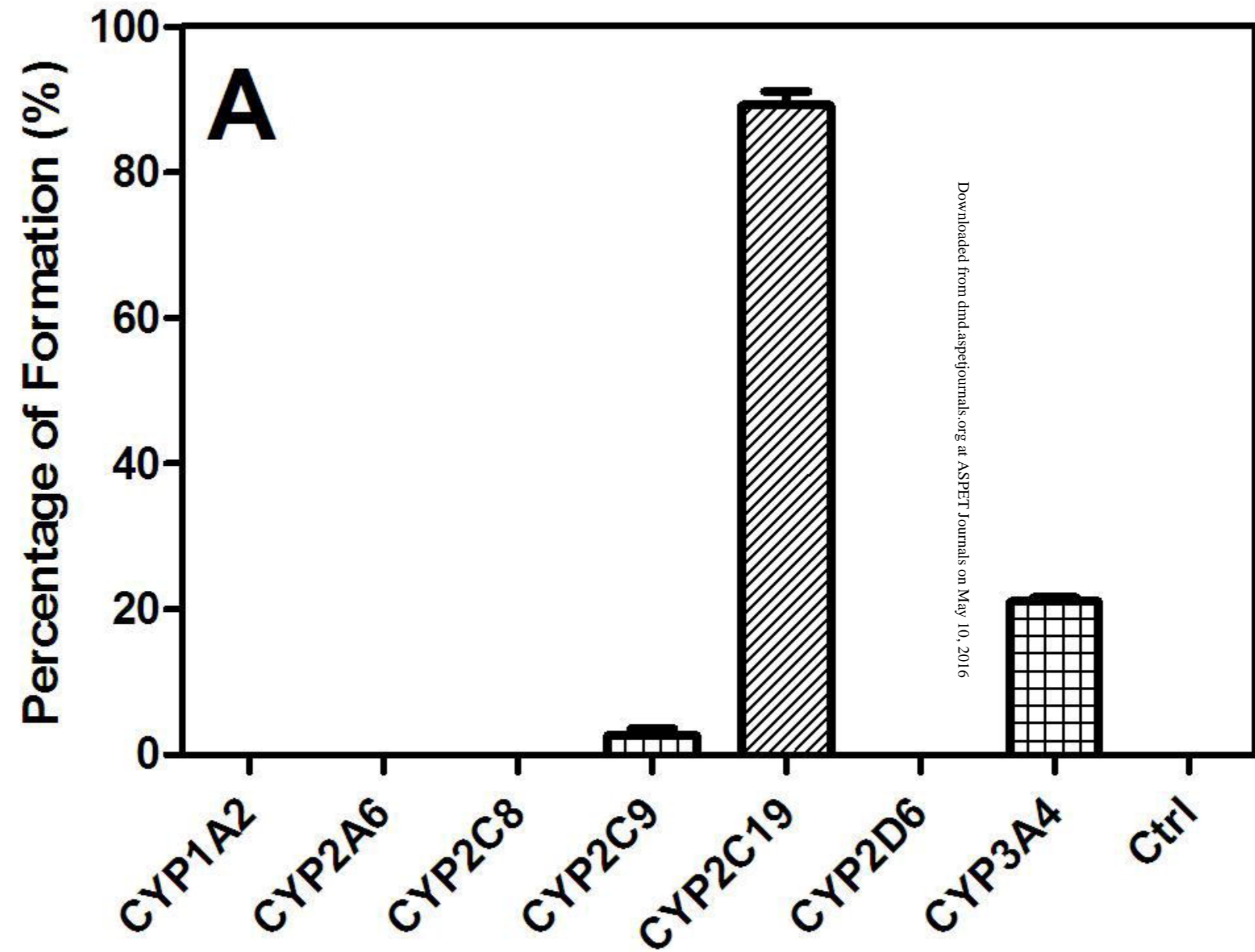


Figure 8

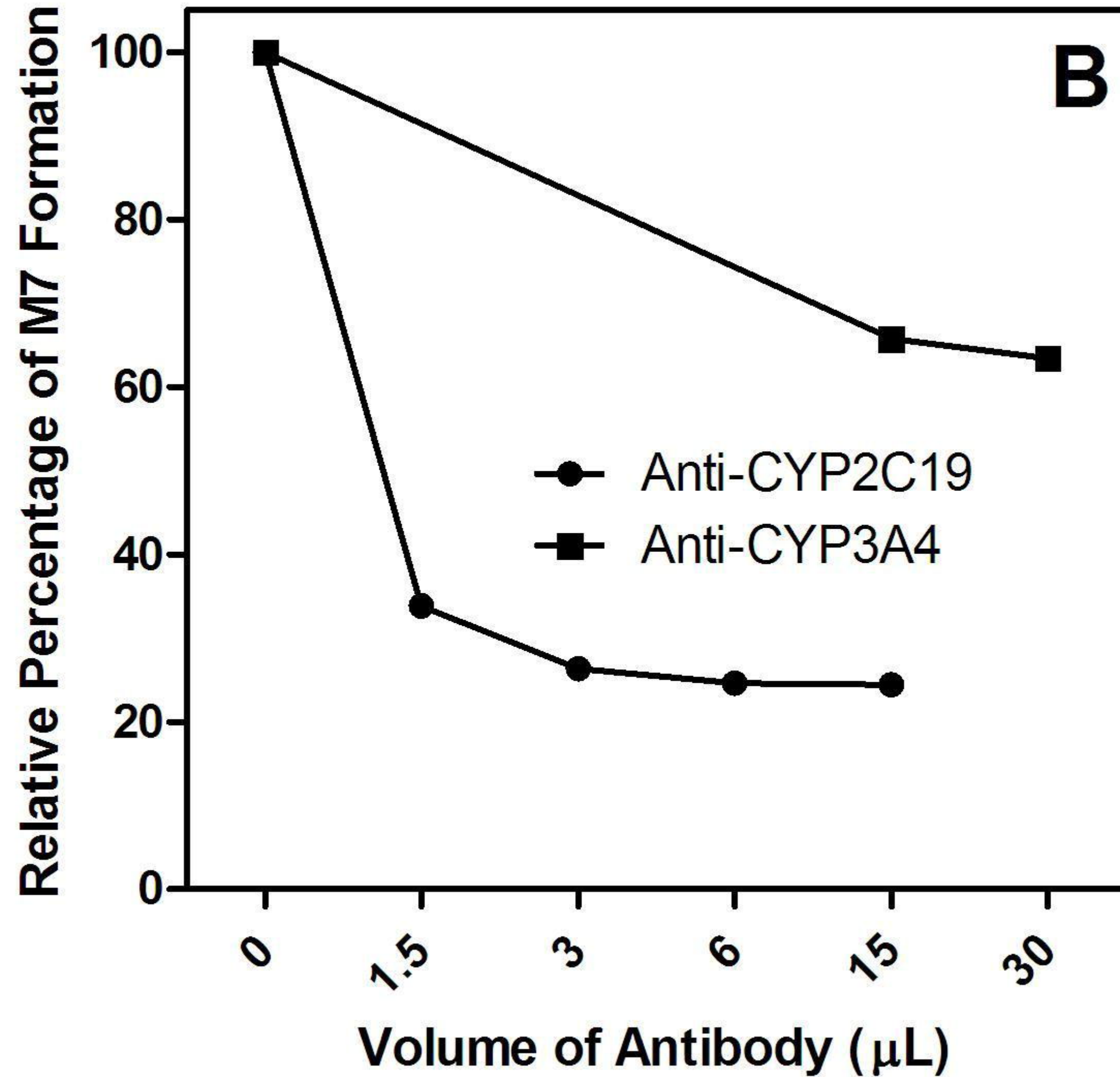
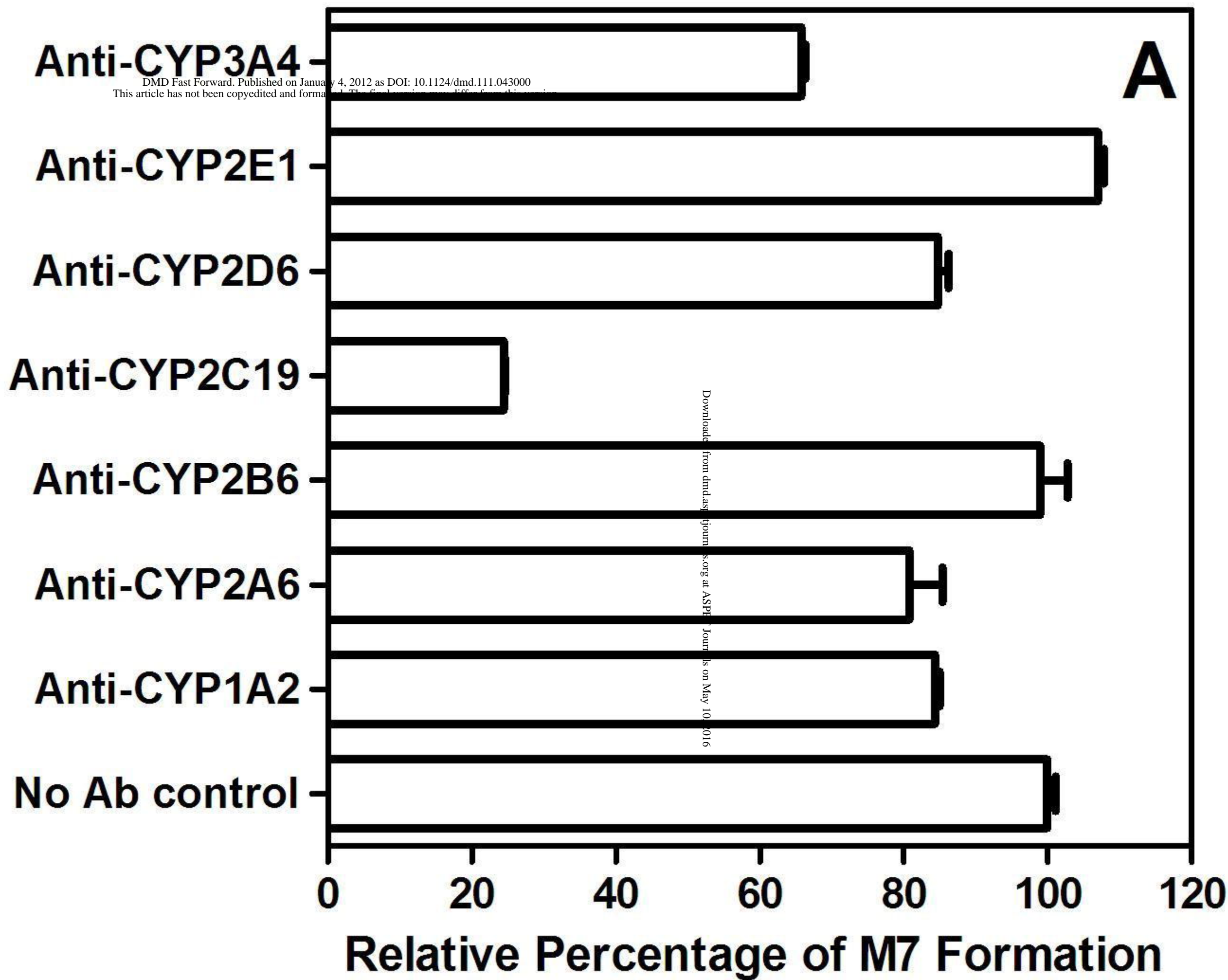


Figure 9

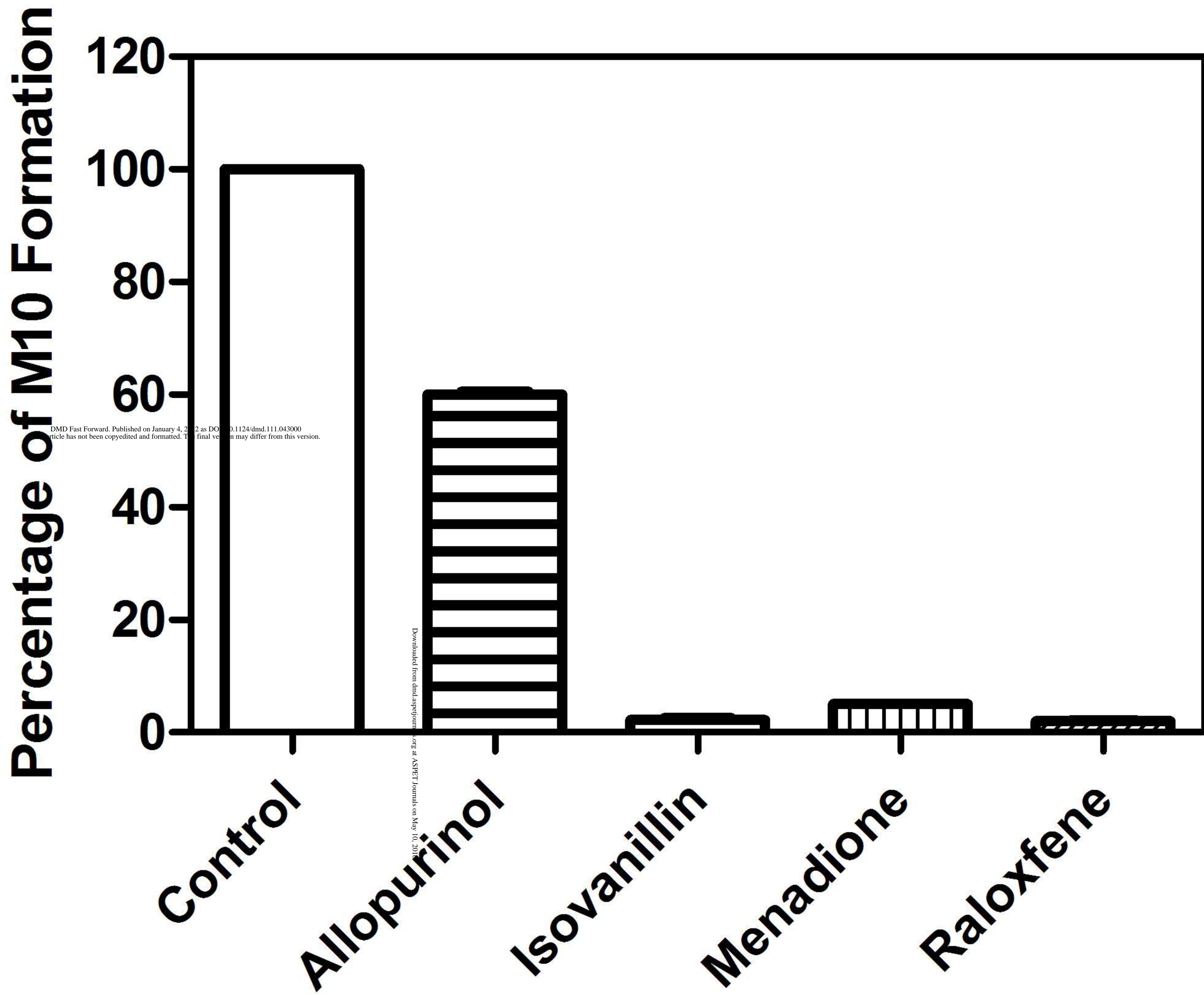
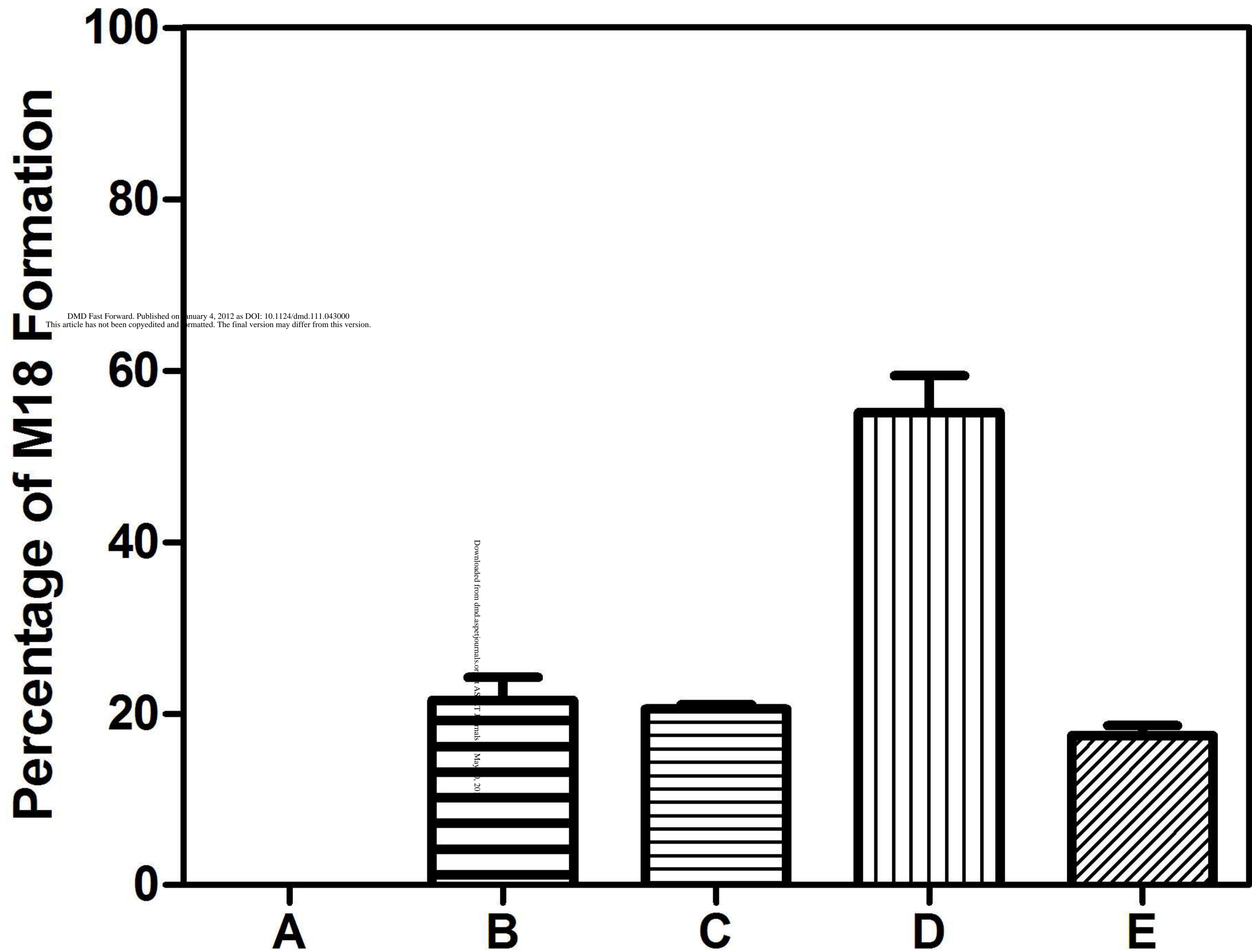


Figure 10



DMD Fast Forward. Published on January 4, 2012 as DOI: 10.1124/dmd.111.043000
This article has not been copyedited and formatted. The final version may differ from this version.

Downloaded from dmd.aspetournals.org at ASU on May 20, 2012

